12-2012

Early Permian Seawater from the delta18O Record Of Fossil Bivalves: Seasonality And A Latitudinal Gradient

James Andrew Beard
Syracuse University

Abstract

The transition from a glaciated world to one that was ice-free makes the early Permian a time interval that in many ways mirrors the present, and hence there is great interest in constraining paleoclimate conditions over that transition. A common method for estimating ancient temperatures uses the oxygen isotope composition of marine carbonate, but this approach becomes significantly more complicated prior to the Cretaceous due to uncertainties about diagenesis and the isotopic composition of seawater, which has been hypothesized to be more depleted than during the Cenozoic. I use stable isotope compositions of sequentially microsampled accretionary calcite from fossil bivalves in SE Australia to evaluate Permian seawater isotope composition and water temperature seasonality. Co-occurring dropstones, diamicts, and glendonites constrain winter temperatures to near-freezing and hence allow calculations of water composition. Records from microsampled specimens of the bivalve *Eurydesma*, spanning roughly 11° of paleolatitude (North Sydney Basin, New South Wales to Hobart, Tasmania) reveal cyclic seasonal fluctuations in $\delta^{18}O_{carb}$ that vary with latitude. The $\delta^{13}C_{carb}$ values exhibit ~1‰ of seasonal variation, and are in agreement with characteristically positive values published for the early Permian of ~5.5‰. The $\delta^{18}O_{carb}$ values vary seasonally by up to 3.3‰around a mean that decreases from -1.2‰ to -1.75‰ moving towards the pole; more enriched isotope values correspond to dark growth bands within the shells, suggesting slower growth in the winter months. Mean $\delta^{18}O$ and seasonal amplitude both decrease with increasing paleolatitude, similar to an observed gradient in the modern high latitudes off the coast of Greenland. Decreasing seasonality is a reflection of decreasing summer temperatures with increasing latitude, while winter temperature minima are presumed to be constant because of freezing conditions. The decrease in mean $\delta^{18}O_{carb}$ with latitude reflects decreasing $\delta^{18}O_{water}$,

similar to that observed over a similar latitudinal range off Greenland today. As with Greenland, the slope of the $\delta^{18}O$-latitude relationship is steeper than that seen in the global ocean today, indicating some contribution of isotopically negative fresh water. Whether this reflects progressive mixing with isotopically negative water from higher latitudes (e.g., the Arctic Ocean today) or similar amounts of runoff/precipitation at each location that itself is progressively more negative with latitude is as yet unclear, though significant departure from marine salinities is not observed.

Early Permian Seawater From The $\delta^{18}O$ Record Of Fossil Bivalves:

Seasonality And A Latitudinal Gradient

By

James Andrew Beard

B.S. University of Tennessee at Chattanooga

THESIS

Submitted in partial fulfillment of the requirements for the degree of Master of Science in Earth Sciences in the Graduate School of Syracuse University

December 2012

Acknowledgements

I thank Bruce Runnegar for his insights, feedback, and for sending additional specimens, Paul Tomascak at SUNY-Oswego for help with the ICP-MS work, David Linsley at Colgate for preparing the thin sections, Jack Hietpas and Melissa Hicks for help interpreting textures in my thin sections, Maddie O'Connor for help sampling my specimens, and numerous students throughout the Syracuse Earth Sciences department who helped provide meaningful discussion related to my work, including; Steve Riccio, Kwasi Gilbert, David Gombosi, Andrew Horst, Aaron Satkoski, and Vicky Wang. I also want to acknowledge the guidance and insight of my committee members Bruce Wilkinson and Scott Samson who have greatly helped improve not only my thesis, but also my skills as a researcher and academic. And last but not least my advisor Linda Ivany who has been an insightful and knowledgeable mentor and teacher for the last 2 years. She has helped make me a better writer, teacher, geologist, and person.

I also want to give a special thanks to my wife who has been with me throughout this entire process and has been an ever supportive figure continuing to encourage me to excel, even through the trials and tribulations of having our first son, James Austin Beard.

Table of Contents

Introduction

Global climate transitioned from an icehouse to a greenhouse state during the early Permian (Li and Powell, 2001; Korte et al., 2005; 2008; Fielding et al., 2006; Clapham and James, 2008). Because continental ice sheets were waning in size, the early Permian offers similarities to waning of modern ice-sheets, and hence there is great interest in constraining paleoclimate conditions over that transition (Fielding et al., 2006;Korte et al., 2008; James et al., 2009; Ivany and Runnegar, 2010). The majority of evidence for deglaciation is contained within the sedimentary record, and detailed stratigraphic, geochemical, and paleobotanical studies have done much to clarify the processes and conditions associated with deglaciation (Dickins, 1978; 1996; Runnegar, 1979; 1980ab; McClung, 1980ab; Herbert, 1980; Rees et al., 2002; Clapham and James, 2008; Fielding et al., 2008; 2010; Frank et al., 2008a; Korte et al., 2008). Quantitative estimates of paleotemperatures through this window, however, are fraught with the uncertainties that accompany studies of the very distant past. Stable isotope compositions of oxygen have proved to be invaluable tools for addressing issues relating to climate in the Cenozoic, but applying this proxy to Paleozoic samples is more difficult. The primary reason for this difficulty is in determining whether or not the specimens have retained their primary isotopic compositions or if they have been diagenetically altered. This concern is further exacerbated by the age disparity between more recent specimens and Paleozoic specimens because of the increased probability of alteration via exposure, diagenetic fluids, or thermal resetting in older samples.

A growing number of authors have used stable oxygen isotopes in the later part of the Paleozoic to interpret climate (Compston, 1960; Lowenstam, 1961; Mii and Grossman, 1994; Veizer et al., 1997; 1999; Wenzel et al., 2000; Korte et al., 2008; Angiolini et al., 2009; Ivany

and Runnegar, 2010; Nützel, 2010; Mii et al. 2012; and others). The vast majority of these studies use shell carbonate of brachiopods and bivalves and report isotope compositions for geographically isolated samples of dozens of individuals, either as shell fragments, bulk specimens, or (more rarely) through high-resolution sampling of individual specimens. While these studies have vastly improved our understanding of conditions during this transition, they nevertheless face the pervasive challenge of demonstrating the primary nature of isotope compositions, and they lack the spatial resolution within individual specimens necessary to address questions of seasonality, a component of climate that is gaining more attention in studies of deep earth history.

Here, I report data from 9 early Permian bivalve specimens sampled sequentially at high spatial resolution within shells. This approach has been widely used in younger specimens to resolve seasonal environmental variation recorded by organisms that produce a carbonate skeleton by accretion (Jones, 1980; Williams et al. 1982; Quitmeyer et al., 1985; Buick and Ivany, 2004; Hallmann et al., 2008; Ivany et al., 2004; Schöne et al., 2004; 2005(a)(b); 2008). Isotope data come from shells of the bivalve *Eurydesma cordatum* (Morris 1845) from SE Australia that span roughly 1100 km of the modern outcrop belt. *Eurydesma* is a cold-water, high-latitude, calcitic bivalve characteristic of the Permian of Gondwana (Runnegar, 1979). Specimen locations range from the North Sydney Basin at ~64°S paleolatitude to the Tasmanian Basin at ~75°S paleolatitude (Scotese, 2002) and are closely associated with sedimentologic and mineralogic indicators of near-freezing conditions. Seasonally resolved records of $\delta^{18}O_{carb}$ not only afford an additional method by which to evaluate the influence of diagenesis on ancient shell carbonate (through preservation of a variable cyclic signal throughout ontogeny), but also provide estimates of paleoseasonality of water-temperatures in the early Permian ocean off the

coast of Gondwana. In addition, by sampling across a wide range of paleolatitudes and from sites with independent evidence for cold temperatures, it is possible to place constraints on regional differences in water composition that might relate to latitudinal gradients associated with the Permian hydrologic cycle.

Geologic Setting and Depositional Environment

During the early Permian, Australia was connected to Antarctica and located close to the South Pole as the southern-most portion of Pangaea (Figure 1) (Li and Powell, 2001; Stampfli and Borel, 2002; Fielding et al., 2010). Sediments from which specimens sampled in this study originate were deposited on a continental shelf atop folded, older Paleozoic rocks. Localities span more than 1,100 km of modern exposure in SE Australia, from northern New South Wales (north Sydney Basin) to Tasmania (Figure 1). Early Permian paleolatitudes for the North and South Sydney Basin span ~64-70°S, while the Tasmanian region was at a latitude of ~73-75°S (Li and Powell, 2000; Stampfli and Borel, 2002; Korte et al., 2008).

Specimens of *Eurydesma* were collected from shallow-water, marine, sedimentary rocks of Sakmarian age that include the pebbly Bundella Mudstone, the volcanogenic sands of the Millfield Farm and Allandale Formations, the sandstones and breccias of the Wasp Head Formation, the medium-fine grained Cranky Corner Candstone, and the biomicritic and dropstone-rich Darlington Limestone (Runnegar, 1979, 1980a; McClung, 1980b; Fielding et al., 2006; Rygel et al., 2008; Ivany and Runnegar, 2010; Australian Government, Geoscience Australia, 2011; Figure 2, Table A1). In addition, the somewhat younger (Kungurian) and deeper-water Wandrawndian Siltstone (Runnegar, 1979, 1980a; Fielding et al., 2006, 2008; Rygel et al., 2008; Ivany and Runnegar, 2010) was also sampled. These units and coeval

formations in the region all contain indicators of cold-water deposition, including tillites, dropstones, and glendonites (De Lurio and Frakes, 1999; Runnegar, 1979; Frank et al., 2008a,b; Selleck, 2007; Suess et al., 1982). The Darlington Limestone in particular contains numerous layers of dropstones, some of which are very large (Runnegar, 1979; Reid, 2010). Glendonites are pseudomorphs after the mineral ikaite; an authigenic hydrated calcium carbonate that forms in sediments at temperatures below 4°C (Bischoff, 1993). Glendonites are common in these early Permian units and constrain depositional temperatures to near freezing (Frank et al., 2008a,b; Selleck, 2007). Common fossils include the epifaunal bivalves *Eurydesma cordatum* and *Deltopecten*, the spiriferid brachiopods *Trigonotreta* and *Ingelarella*, and hard-substrate-encrusting trepostome bryozoans (Runnegar, 1979; Reid, 2010). A number of semi-infaunal and infaunal bivalves, crinoids, rugose corals, and gastropods are also present (Runnegar, 1979, 1980b; McClung, 1980a; Reid, 2010; Clapham and James, 2008) (Table A1). This community of organisms is representative of open marine conditions and therefore normal marine salinity (Clapham and James, 2008).

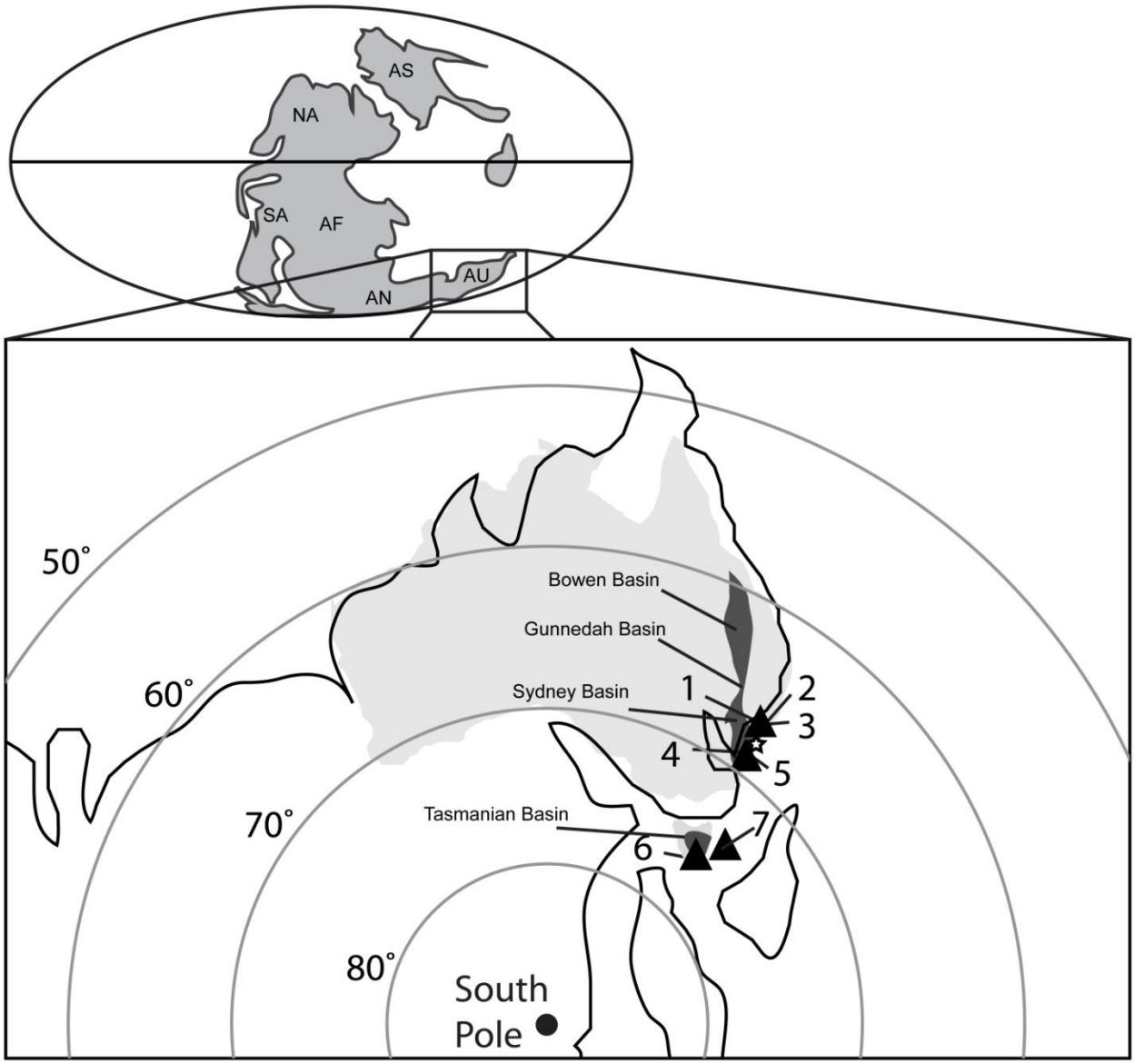

Figure 1) Paleogeographic reconstruction showing the approximate locations of sample sites (1. Allandale Railroad, 2. Bimbadeen, 3. Cranky Corner and Tangorin, 4. Wasp Head, 5. North Head, 6. Derwent River, 7. Maria Island). Sydney-Gunnedah-Bowen and Tasmanian Basin systems are indicated by dark shading, and present-day outline of Australia is in pale gray. Modified from Blakey (http://cpgeosystems.com/index.html) and Mii et al. (2012).

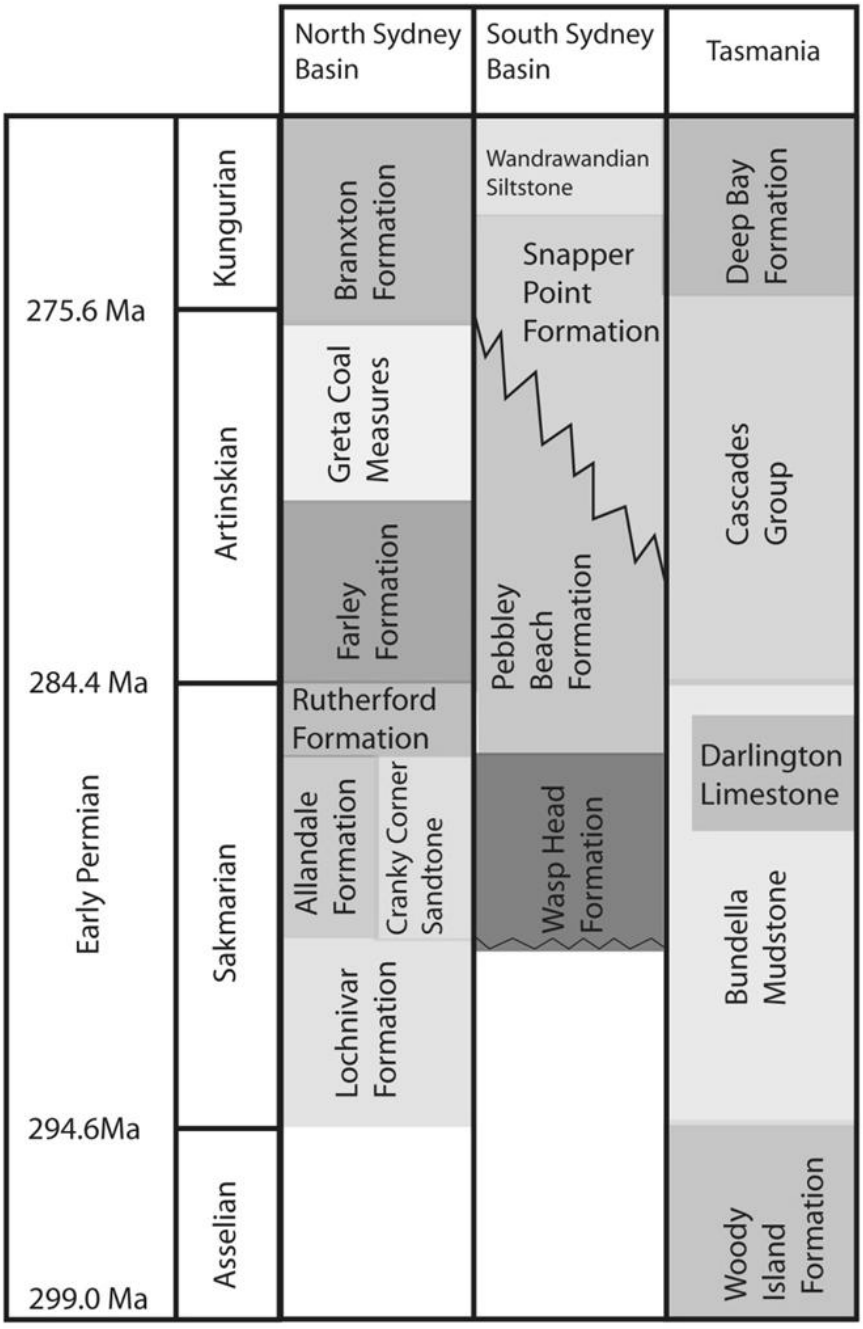

Figure 2) Stratigraphic sections of the three regions sampled in this study. Specimens mostly come from Sakmarian equivalents of the Allandale Formation. Based on information derived from Runnegar (1979, 1980b); McClung (1980a); Ivany and Runnegar (2010); Reid (2010); Reid and James (2010); Rygel et al. (2008); Fielding et al. (2006); Geoscience Australia; and Runnegar (personal communication). See Table A1 for details.

Eurydesma cordatum

Eurydesma was an immobile epifaunal bivalve with massive, heavily calcified umbones that acted as an anchor to help it maintain its preferred hinge-down orientation in high energy environments with low sedimentation rates (Runnegar, 1979). While its specific taxonomic affinity is uncertain, it belongs to the Subclass Pteriomorphia, the group that includes the oysters, marine mussels, pectens, and arcs (Runnegar 1979). Specimens of *Eurydesma* provide an ideal platform for this study. First, the shells of *Eurydesma* are composed of diagenetically stable, low-Mg calcite, and the thick and heavily calcified umbones offer well defined and expanded growth lines for sampling (Figure 3). Secondly, bivalves are known to precipitate calcite in isotopic equilibrium with water (e.g. Mook and Vogel, 1968; Klein et al., 1996), making paleotemperature reconstruction possible. Earlier work for *Eurydesma* has shown that alternating light and dark growth bands are seasonal, with the lighter colored regions exhibiting periods of faster growth during the warmer months and darker regions representing periods of slower growth and/or growth cessation (Ivany and Runnegar, 2010).

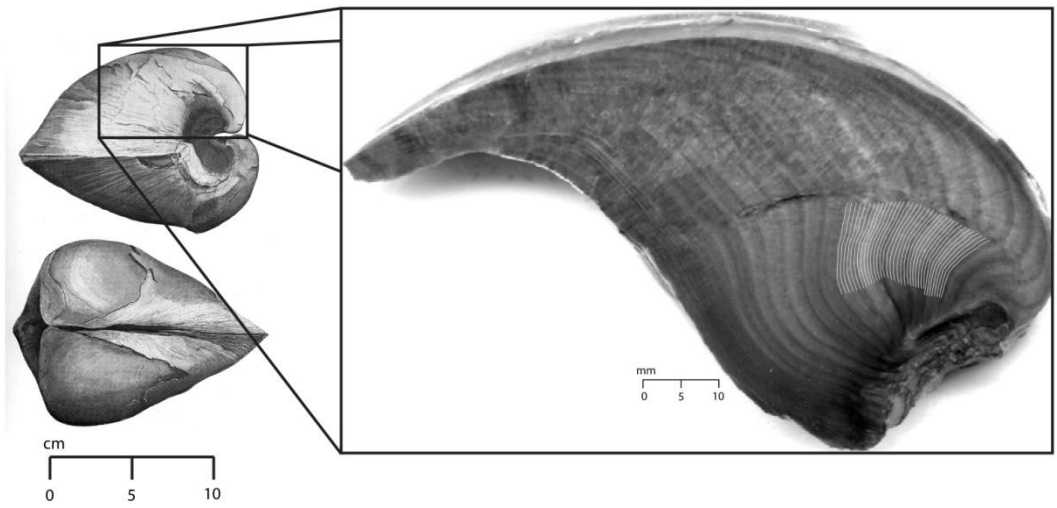

Figure 3. *Eurydesma cordatum* modified from Morris (1845), with inset showing cross section through the umbo of specimen MIsA from Maria Island, Tasmania. Digitized sampling lines are superimposed on growth banding.

Methods

Specimens were cut through the umbo perpendicular to growth and polished to reveal growth banding. Thin sections were prepared for the examination of shell textures, and thick sections were prepared from the immediately adjacent slab for micromilling. Three or more spot samples were collected from each thick section for evaluation of diagenetic alteration using minor element (Fe, Mn) concentrations; analyses were carried out using the quadrupole ICP-MS at SUNY-Oswego. Thick sections were spot sampled for initial evaluation of stable isotope values, and 8 shells were micromilled at a resolution of 6 samples per year over 5 consecutive years. Sampling was done in the central region of the umbo to minimize potential exposure to diagenetic fluids, and near the faster-growing, juvenile portion of the ontogeny so as to exploit the more expanded growth lines and hence better temporal resolution. Any evident cracks or microborings were avoided, but several samples from obviously secondary cements filling such structures at or near the exterior surface of shells were collected for comparison with shell

isotope values. Stable isotope analyses ($\delta^{18}O$ and $\delta^{13}C$) were performed at the University of Kansas using a Finnigan MAT 253 isotope ratio mass spectrometer coupled to a KIEL III automated carbonate reaction device.

Results

Textures in Thin Section

Thin sections reveal shell fabrics with prismatic elongate calcite crystals oriented perpendicular to the growth banding (Texture A in Figure 4). Crystals exhibit undulatory extinction, and microgrowth increments similar to primary shell textures as seen in other pteriomorph bivalves such as *Pinna bicolor* (Carter and Stehli, 1980). A second fabric of smaller 'bushy' calcite crystals oriented parallel to growth-band-parallel features within the shell (Texture B in Figure 4) is also observed within some of the specimens. Texture B is interpreted as a primary feature related to a change in growth rate, as the fabric is concentrated on the commissure side of the growth-parallel features and would be expected to be distributed on both sides if simply diagenetic.

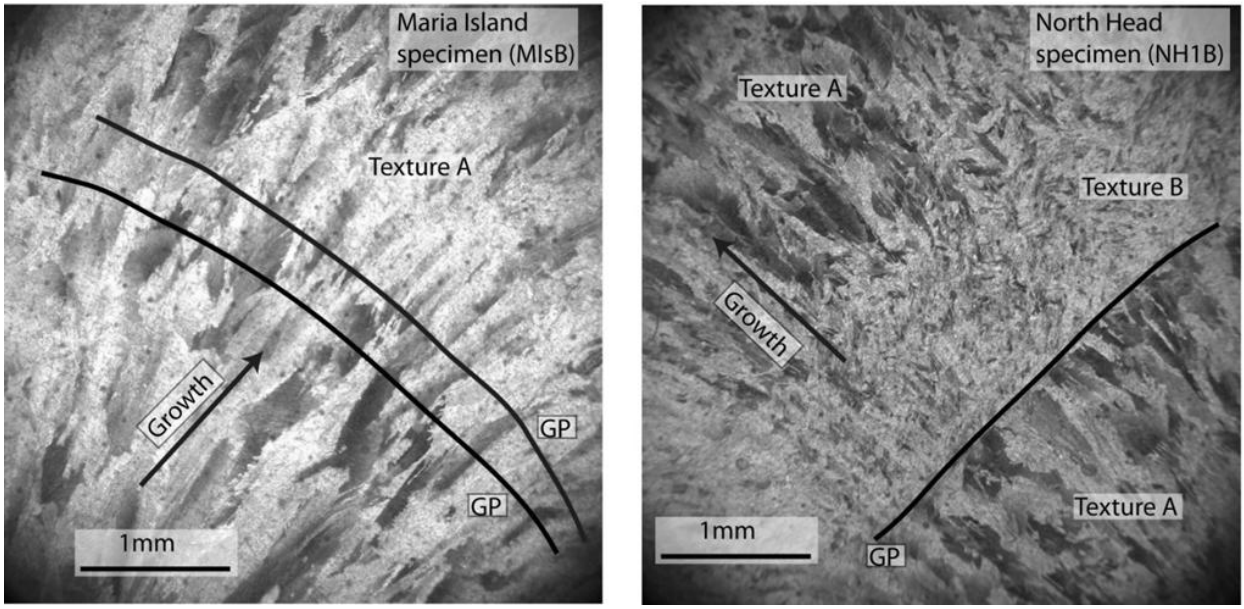

Figure 4. Photomicrographs of two *Eurydesma* specimens in plane-polarized light. GP = Growth-parallel crack, Texture A = Prismatic elongate crystals oriented parallel to the direction of growth, Texture B = Smaller 'bushy' crystals randomly-oriented and associated with growth-parallel features

Elemental Geochemistry

Concentrations of Fe and Mn have been widely used to indicate alteration of shallow marine carbonates (Morrison and Brand, 1986; Brand, 1989; 2004; Brand et al. 2003; Korte et al., 2008; Mii and Grossman, 1994; Mii et al., 2012; Wenzel, 2000). Fe and Mn are often enriched in marine carbonates during diagenesis due to the tendency for those elements to be present at higher concentrations in pore water under anoxic conditions (Brand, 1989). Shell samples from *Eurydesma* plot within the range reported for well-preserved Permian bivalves and brachiopods (Mii et al., 2012; Korte et al., 2008), and modern brachiopods from Brand et al. (2003) (Figure 5, Table A2). A range of threshold values for Fe and Mn concentrations in calcite have been proposed by numerous authors above which diagenetic alteration is to be

suspected. In this study, we use conservative values of Mn <300ppm and Fe <1,000ppm (Morrison and Brand, 1986; Brand, 1989; Korte et al., 2008) to indicate primary shell carbonate. The 4 samples exhibiting values of Mn >300ppm and/or Fe >1,000ppm are cements on the exterior of a specimen from Maria Island, a sample from within a crack in a Maria Island specimen, and a microbored region of the North Head specimen, all collected for comparison with samples from the central region of the umbo where stable isotope sampling was done. Samples from umbonal regions exhibit Fe and Mn concentrations of 66±67ppm and 11±4ppm, respectively, well within the suggested limits for primary shell, and many were at or below the detection limit for Fe at 5ppm.

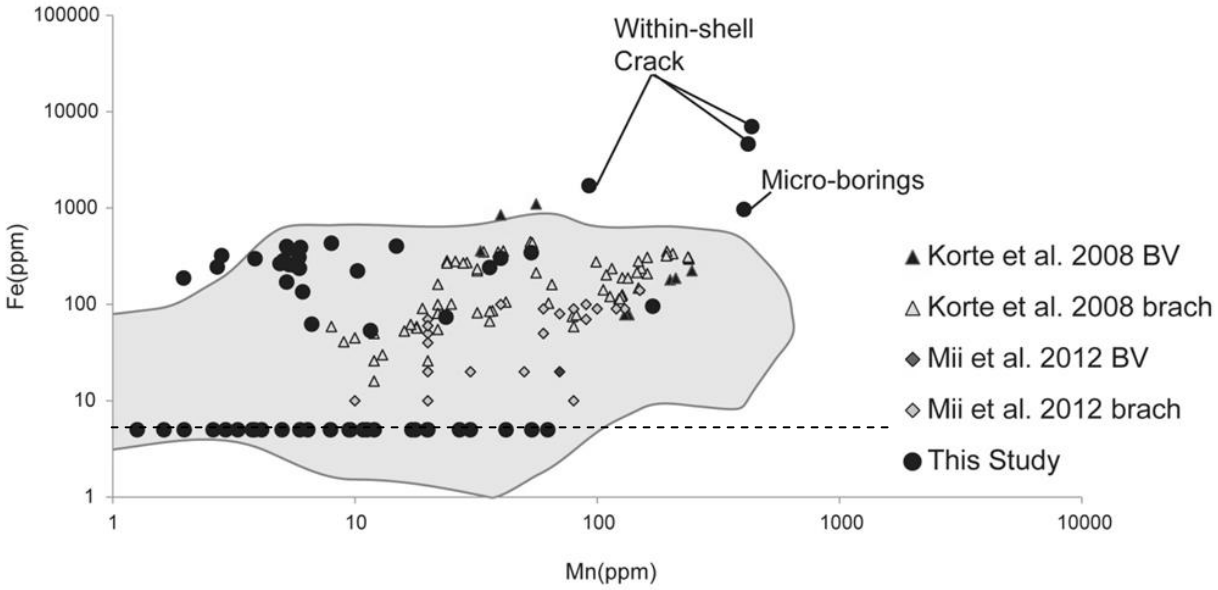

Figure 5. The concentrations of Fe and Mn from *Eurydesma* (solid black dots) and published data from other well-preserved Permian bivalves and brachiopods. The gray field represents the region occupied by modern brachiopods from Brand et al. 2003. Fe and Mn concentrations >1,000 ppm and >300 ppm respectively were used in this study as indicators of suspected alteration, and the dashed line is the detection limit for Fe.

Stable Isotopes

Plots of isotope value versus distance along the sampled shell define cyclic variation in $\delta^{18}O_{carb}$ in all but one of the specimens, as expected for shell accretion during seasonal fluctuations in temperature (Figure 6). Values of $\delta^{18}O_{carb}$ range from ~1‰ and -3 ‰, and growth bands are associated with positive isotope values and hence winter months (Table A3). A single specimen from Derwent River yields somewhat more negative values (-2.9‰ to -5.1‰ with an average of -3.8‰) and does not exhibit obvious seasonal variation. Carbon isotope compositions within specimens show substantially less variation, a weak tendency to co-vary positively with oxygen isotope values, and hover near the published values of around +5.5‰ for the Permian open ocean (Mii et al., 1997; Grossman, et al., 2008; Veizer et al., 1999), ranging from +4.0 to +6.3‰ (Figure 6).

Mean winter values for each shell are computed from the most positive oxygen isotope values within each annual cycle (4-6 winters per shell), mean summer values from the most negative (3-7 summers per shell), and seasonal range from the difference between these two, with the exception of the Derwent River specimen (Table 1). Mean winter $\delta^{18}O_{carb}$ values decrease with increasing latitude, ranging from 0.88‰ ±0.34‰ for the Bimbadeen specimen in the North Sydney Basin to -0.96‰ ±0.33‰ for the Maria Island 1 specimen in the Tasmanian Basin, ($r^2 = 0.70$; Figure 7). There is no latitudinal trend in mean summer values (North Sydney Basin average = -2.53‰ ± 1.37‰ Tasmania = -2.44‰ ± 0.26‰). The seasonal range of $\delta^{18}O$ values, therefore, generally decreases with increasing latitude, but the trend is not without exception, as summer $\delta^{18}O$ values are more variable among locations (Table 1 and Figure 8).

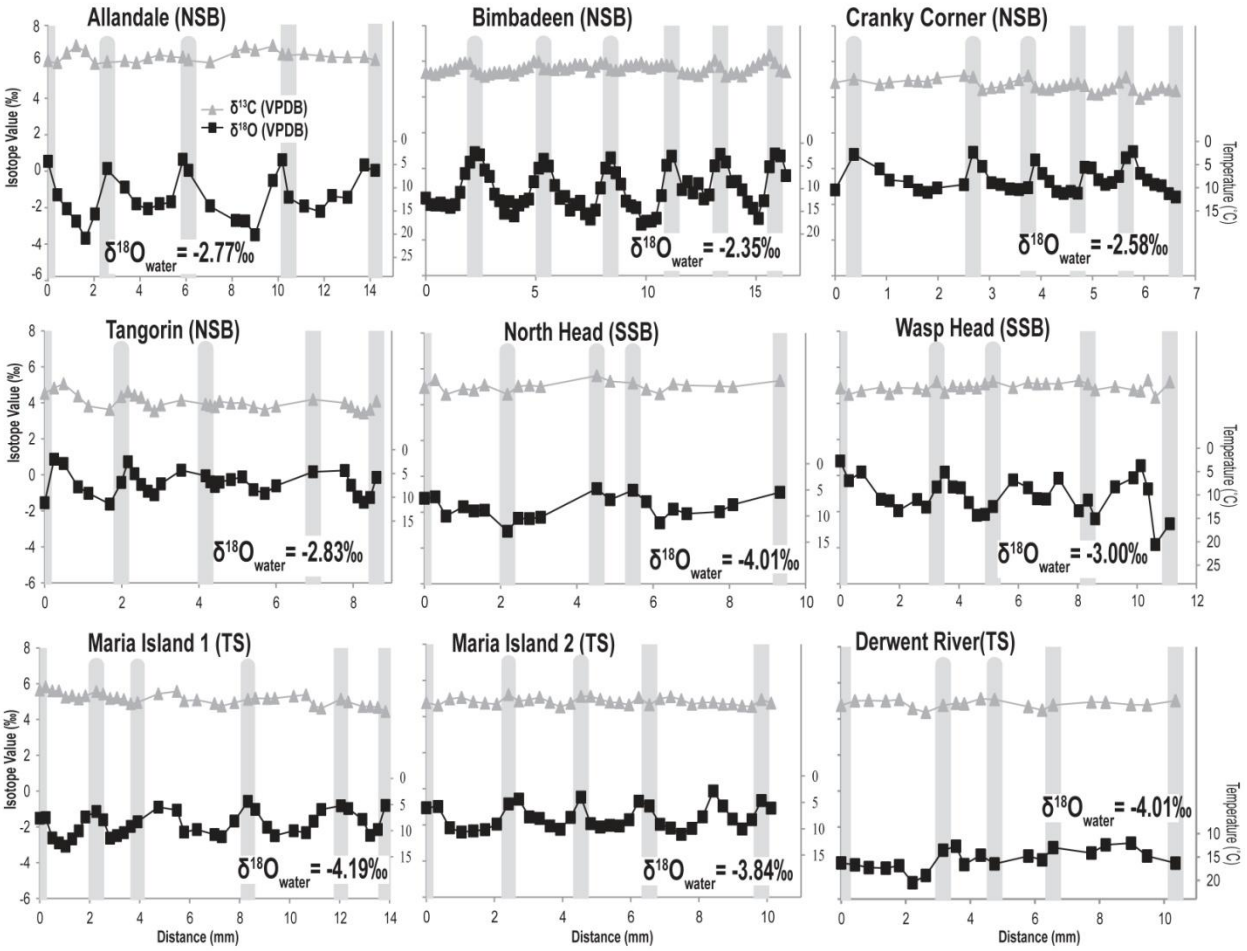

Figure 6. Plots of $\delta^{18}O$ and $\delta^{13}C$ versus the position in the shell and the inferred temperature for each of the specimens sampled in this study plus a published specimen from Bimbadeen (Ivany and Runnegar; 2010). Temperatures for each specimen are determined using a $\delta^{18}O_{water}$ calculated assuming a winter minimum of 4°C (see text for details).

Table 1. Mean shell isotope values by paleolatitude.

Basin	Locality	Summer $\delta^{18}O_{carb}$	Mean Summer	Winter $\delta^{18}O_{carb}$	Mean Winter	Seasonality	Mean Seasonality	Midpoint (season average)
NSB	Allandale	-3.67	-2.85	0.54	0.46	4.21	3.35	-1.19
		-2.06		0.15		2.21		
		-3.48		0.65		4.13		
		-2.20		0.63		2.83		
				0.35				
NSB	Bimbadeen	-1.85	-2.31	1.11	0.88	2.96	3.19	
		-2.43		0.24		2.67		
		-2.61		0.81		3.42		
		-2.90		0.91		3.81		
		-1.48		1.20		2.68		
		-2.58		1.03		3.61		
NSB	Tangorin	-1.55	-1.24	0.87	0.40	2.42	1.59	-0.42
		-1.62		0.73		2.35		
		-1.10		0.26		1.36		
		-0.64		-0.11		0.53		
		-1.03		0.24		1.27		
		-1.52						
NSB	Cranky Corner	-1.19	-1.26	0.80	0.65	1.99	1.84	-0.31
		-1.33		0.91		2.24		
		-1.17		0.49		1.66		
		-1.39		0.08		1.47		
		-0.89		0.95		1.84		
		-1.59						
SSB	Wasp Head	-1.95	-2.33	0.81	0.23	2.76	2.56	-1.05
		-2.20		0.19		2.39		
		-1.30		-0.24		1.06		
		-2.39		-0.15		2.24		
		-3.82		0.55		4.37		
SSB	North Head	-2.21	-2.62	-1.14	-0.87	1.07	1.76	-1.75
		-3.06		-0.68		2.38		
		-2.59		-0.77		1.82		
				-0.89				
TS	Maria Island 1	-3.08	-2.55	-1.51	-0.96	1.57	1.60	-1.75
		-2.63		-1.14		1.49		
		-2.28		-0.89		1.39		

		-2.55		-0.57		1.98		
		-2.49		-0.82		1.67		
		-2.32		-0.80		1.52		
		-2.47						
TS	Maria Island 2	-2.39	-2.29	-0.98	-0.61	1.41	1.68	-1.45
		-2.20		-0.57		1.63		
		-2.11		-0.46		1.65		
		-2.52		-0.90		1.62		
		-2.23		-0.12		2.11		
				-0.65				

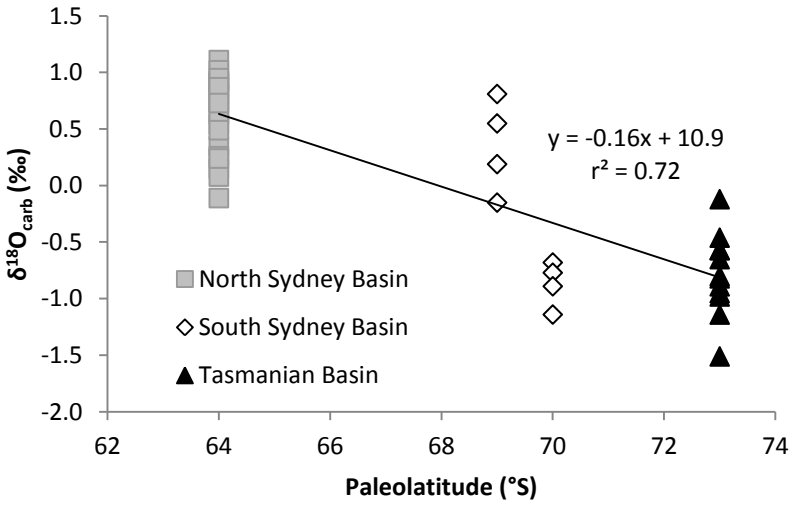

Figure 7. Minimum $\delta^{18}O$ values for each winter season of each shell plotted by paleolatitude.

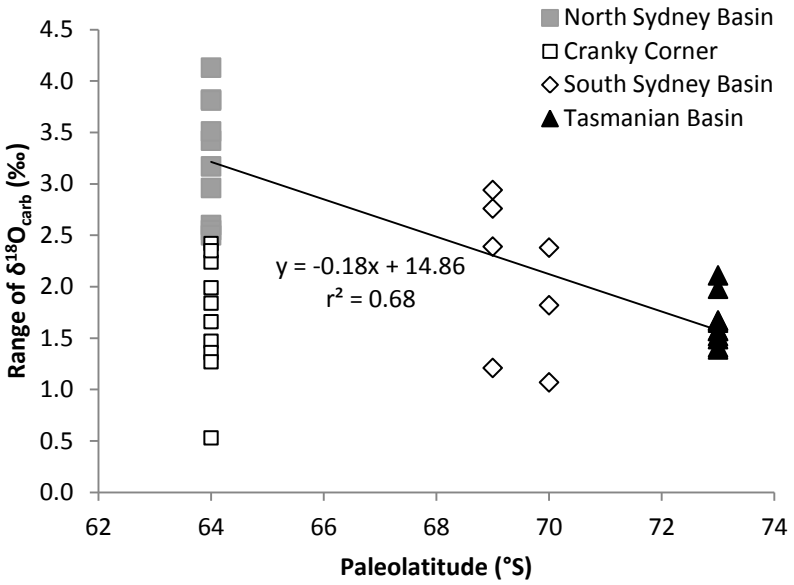

Figure 8. Seasonal range of $\delta^{18}O$ values with latitude. (Note that both samples from the Cranky Corner sandstone are not included in the regression)

Discussion

Primary signal or diagenesis?

Critical to any paleoenvironmental interpretation based on stable oxygen isotope data is the ability to establish whether $\delta^{18}O_{carb}$ values are primary and have not been altered during diagenesis. Shell microtextures and trace elemental concentrations are standard tools by which to identify diagenetic changes. Beyond this, sufficiently depleted oxygen isotope values may give cause for concern, but many otherwise pristine shells with minimal Fe or Mn from the Paleozoic yield surprisingly depleted $\delta^{18}O_{carb}$ values (Veizer et al., 1997; 1999; Brand, 2004), although some have been shown to be altered (Mii and Grossman, 1997). The observed trend toward more negative $\delta^{18}O_{carb}$ values with increasing age has led some to suggest secular change in the oxygen isotopic composition of the world oceans (Veizer et al., 1997), but this is still a contentious hypothesis (see review by Jaffrés, 2007). In this study, *Eurydesma* shell textures are largely consistent with those observed in living bivalves (Carter and Stehli, 1980), and samples

of umbonal calcite exhibit Mn and Fe concentrations well within the range of modern calcitic bivalves and below the typical thresholds for alteration at 300ppm and 1,000ppm, respectively (Morrison and Brand, 1986; Brand, 1989). It is also the case that concentrations of Fe are influenced by other factors, as outlined in Morrison and Brand (1986), and moderately elevated concentrations may not indicate alteration. Stable isotope values are clustered in the most positive portion of the range of published Permian values (Figure 9), consistent with primary values. Clear seasonal variation associated with growth banding is present in all but one specimen, also arguing for the retention of primary compositions (Ivany and Runnegar, 2010). It is therefore unlikely that diagenetic alteration has been significant.

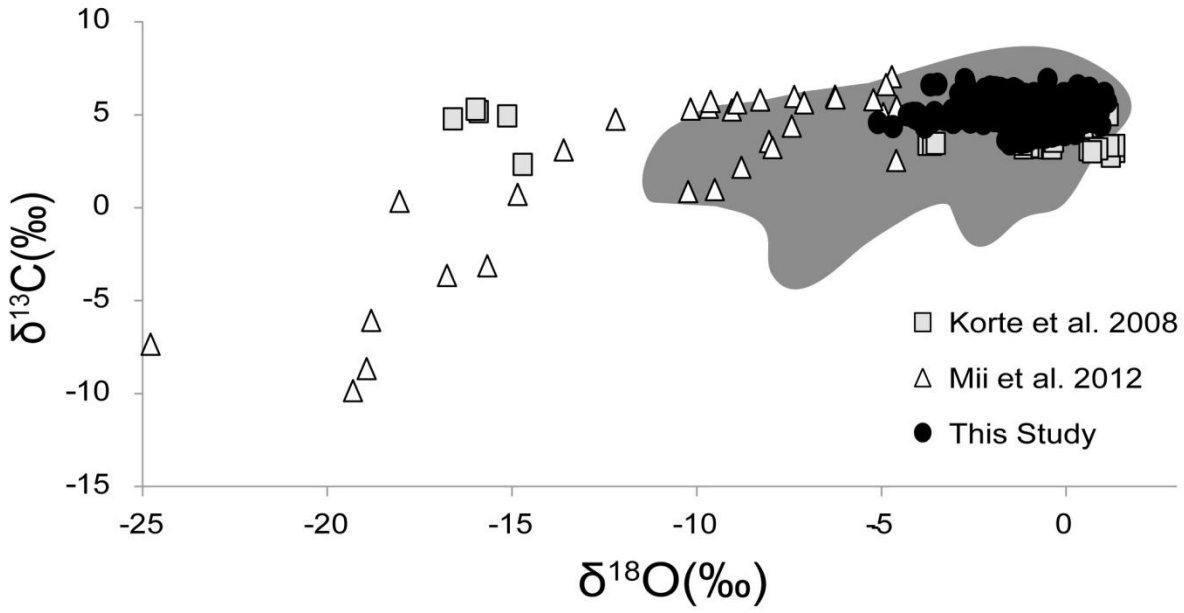

Figure 9. *Eurydesma* $\delta^{18}O$ and $\delta^{13}C$ values from this study (black dots) in comparison to published Permian bivalve data. Shaded region encloses Permian (Mii et al., 2012; Korte et al., 2008) and modern (Brand et al., 2003) brachiopod data. Our data cluster tightly at the most positive end of both axes, whereas progressive diagenetic alteration will shift compositions toward more negative values (Lohmann, 1988).

Paleotemperatures and Water Composition

If shell compositions are primary, they offer the potential to calculate the temperature of the Permian ocean off SE Australia so long as a reasonable value for the $\delta^{18}O_{water}$ can be obtained. Given that these early Permian bivalves were growing at a time when Gondwana was still in part glaciated (Fielding et al. 2008; 2010), we assume that $\delta^{18}O_{water}$ was close to the global average today of 0‰. The resulting temperatures, as calculated from the Epstein et al. (1953) equation for mollusk calcite revised by Anderson and Arthur (1983), range from 20°C for the lowest latitudes and 24°C for the highest latitudes. Not only do these temperatures suggest increasing warmth with latitude, but they are far warmer than that presumed for ikaite formation (≤4°C) and stand in stark contrast with associated cold-water indicators such as tillites and dropstones in these sections (Frank et al., 2008a,b; Selleck, 2007). It therefore seems apparent that the local $\delta^{18}O_{water}$ at these sites was more depleted than 0‰, and that its isotope value likely decreased with increasing latitude, so as to yield temperatures consistent with sedimentologic indicators and the expected trend toward cooler temperatures with latitude that pervades on Earth today.

We therefore calculate local seawater isotope compositions using the isotopic compositions of shell accreted during winter seasonal extremes and assuming that water temperatures were near-freezing at those times (e.g. Ivany and Runnegar, 2010). *Eurydesma* growth was probably restricted to a consistent minimum growth temperature associated with taxon-specific physiological constraints (Schöne et al. 2008); therefore, the winter temperatures recorded are likely to be about the same at each locality. Winter temperature minima in the ocean do not generally fall below -2°C because this is the point at which seawater of typical marine salinity (~35ppt) freezes. Modern Arctic bivalves studied by Schöne et al. (2005b) are

able to grow down to temperatures of 4°C, and the bivalve *Laturnula* living off the coast of Antarctica grows at temperatures between 0° and 3°C (Sato-Okoshi and Okoshi, 2008). The ikaite precursor to co-occurring glendonites is unstable at temperatures in excess of 4°C (Bischoff et al., 1993). Together, these observations suggest that temperatures recorded by *Eurydesma* during the Permian Australian winter likely were in the range of 0-4°C. Solving for $\delta^{18}O_{water}$ using the range of 0 to +4°C and the minimum winter shell compositions yields local water compositions ranging from a maximum of -2.4‰ at Bimbadeen at the lowest latitudes (assuming a maximum precipitation temperature of 4°C) to a minimum of -5.3‰ for Maria Island 1 at the highest (assuming a minimum precipitation temperature of 0°C; Table 2, Figure 10). Regardless of temperature, the gradient in seawater isotope values exhibits a slope of -0.16 per mil per degree latitude with an $r^2 = 0.82$ (Figure 11).

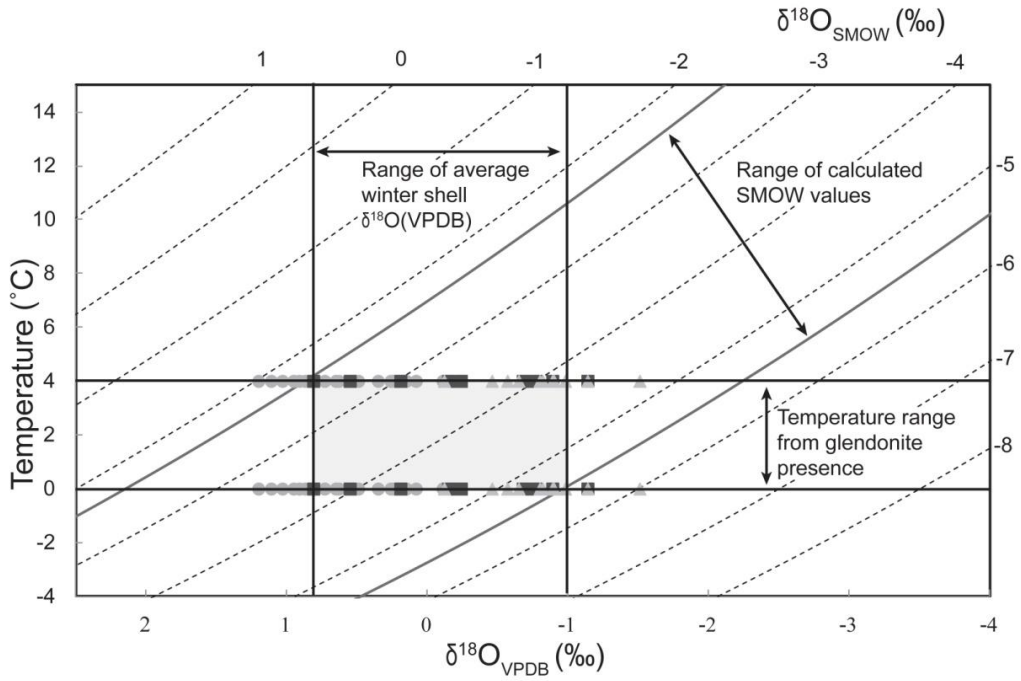

Figure 10. Winter temperatures (0 to 4°C, horizontal lines) used to estimate water isotope compositions (dashed lines) using shell isotope values. The range of average winter shell $\delta^{18}O$ values (in black) span the most positive values at Bimbadeen and the most negative at Maria Island. Gray circles are individual winter values of shell carbonate from the North Sydney

Basin, black squares are from the South Sydney Basin and the triangles are from Maria Island, Tasmania (see Table 1). Local water composition therefore ranged from ~-2.6 in the north when assuming maximum precipitation temperatures of 4 °C to ~-5.3‰ in the south if assuming minimum precipitation temperatures of 0 °C (solid curves).

In the modern ocean, high-latitude surface-water compositions are more depleted than the global mean due to the influence of progressively more depleted precipitation with increasing latitude (Schmidt et al., 1999; Bowen and Wilkinson, 2002; Legrande and Schmidt, 2002). All open-ocean values, however exceed ~ -1.0‰, except where influenced by mixing with the semi-restricted Arctic Ocean, which receives isotopically depleted fresh water during summer melting of polar ice and snow (Ekwurzel et al. 2001). Inferred Permian local seawater values are significantly more negative, and the gradient with latitude is similar to that seen off of the coast of Greenland today (Figure 11), suggesting that Greenland might be a good analog for SE Australia during the Permian. The Greenland latitudinal trend in water composition likely reflects the mixing of depleted meteoric water with seawater. Depleted waters could be admixed from the Arctic Ocean or derived from more local precipitation and/or glacial meltwater. If the latter, the compositional gradient with latitude could be a coincidence of more precipitation/runoff of similar composition to the north, or roughly comparable amounts of isotopically more negative water toward the north. This latter hypothesis is supported by consistent salinities with latitude, averaging ~33 ppt. The influx of fresh water cannot be enough to cause an appreciable drop in salinity, and hence must be isotopically negative enough to effect the change in $\delta^{18}O_{water}$ values without impacting paleoecology. Similar phenomena likely gave rise to the Permian trend as well. However, inferred isotope values of Permian seawater are ~3‰ more negative than the waters off Greenland today, despite similar amounts of change with latitude. Is this offset simply a coincidence of proportionally greater contributions of meltwater

to the Permian coastline than Greenland sees today? Assuming Permian oceans were not unlike those today and marine isotope values at ~65°S were roughly -0.5‰, a mixture with a salinity of approximately 29-32ppt (roughly 9-17% freshwater) would result from the addition of enough fresh water at -30‰ to yield the inferred water values of -3.0 to -5‰. If taxa in the *Eurydesma* fauna were tolerant of salinities in this range, then paleoecologic indicators would not be sensitive enough to reflect brackish conditions. Brachiopods, echinoderms, corals, and bryozoans, however, are generally thought to be stenohaline organisms.

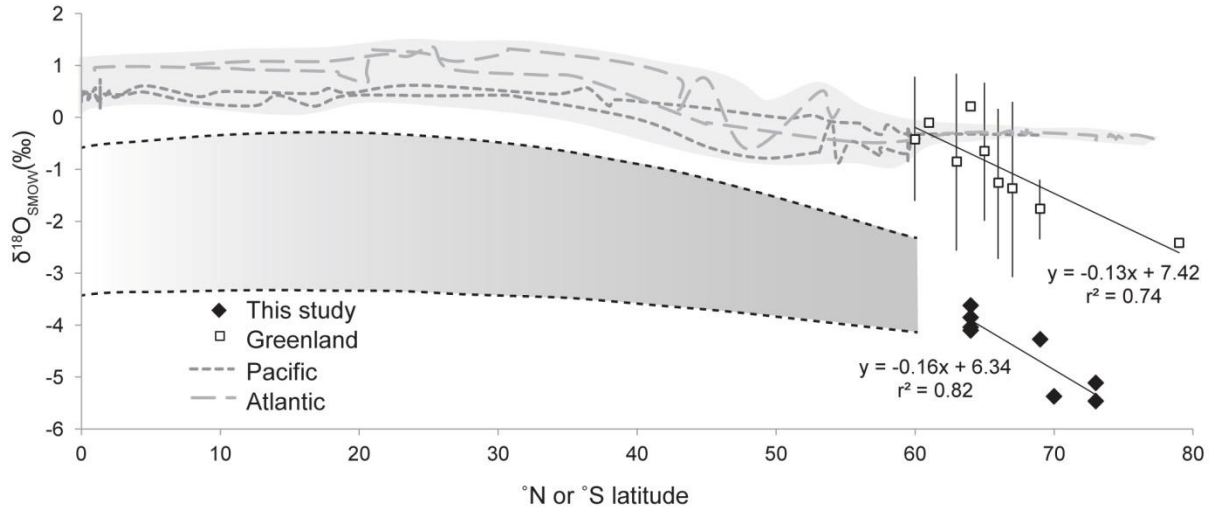

Figure 11. Permian local seawater compositions (calculated assuming a winter minimum of 4°C) versus paleolatitude (black diamonds), and observed compositions for the Pacific, Atlantic, and along the SE coast of Greenland plotted against latitude. The gradationally-shaded region is Permian seawater composition extrapolated from trends in the modern $\delta^{18}O$ values (gray curves) and Permian low-latitude brachiopods. Modern data from the Global Seawater Oxygen-18 Database at NASA, http://data.giss.nasa.gov/o18data/.

The extrapolation shown in Figure 11 is an estimate for low-latitude Permian seawater isotopic composition based on the 2nd order polynomials fit to the modern data but adjusted for the more negative Permian high latitudes, assuming today's Greenland and Permian SE Australia experience similar amounts of runoff. This admittedly tenuous extrapolation suggests tropical

$\delta^{18}O_{water}$ values between roughly -1‰ and -3‰. Published low-latitude $\delta^{18}O_{carb}$ values (Korte et al., 2005) combined with the assumption that Permian tropical temperatures were comparable to those today (~27° C) are consistent with tropical $\delta^{18}O_{water}$ values of around -1‰, at the more enriched end of our estimate. While a tropical seawater value of -1‰ is not far from the global mean today and is within the range of values experienced by the ocean during the Cenozoic, the tropics tend to be more positive than the global mean due to evaporative enrichment of surface waters. A global mean of -1‰ already requires the absence of measurable glacial ice on the planet, and we know that this was not the case during the early Permian. If indeed -1‰ is more positive than the overall mean, and if there was still substantial, if waning (Fielding et al., 2006) glacial ice on Gondwana, it is likely that global mean seawater composition was more depleted than -1‰. There is, however, a considerable amount of uncertainty in this estimate, and that uncertainty may well encompass seawater values more consistent with constant seawater $\delta^{18}O$ through time. At present, we are not able to resolve this uncertainty.

Permian Seasonality

Local Permian water compositions calculated using estimated winter minimum temperatures allow for an approximation of the seasonal range of temperatures in each specimen, so long as local $\delta^{18}O_{water}$ is not changing during the year. Seasonality is greater at lower latitudes, with the North Sydney Basin averaging between 11-12°C and the Tasmanian Basin 5-6°C (Table 2). Because winter temperatures are assumed to be the same across latitude, the decrease in seasonal range with increasing latitude is due to either a drop in summer temperatures toward the pole or increased amounts of run-off at the lower latitudes in the summer. This temperature range is similar to that in today's oceans above ~40°N or S latitude, although Permian seasonal ranges are a bit higher than those at similar latitudes today if water

compositions are constant year-round (Appendix figure A1). Because seasonal range at high latitudes is controlled by summer water temperatures, these data suggest that Permian summers were warmer than those today at similar latitudes, or that increased runoff at the lower latitudes makes this appear so. Given the typical truncation of winter minima and summer maxima pointed out by Williams et al. (1982) and addressed by Wilkinson and Ivany (2002) and Goodwin et al. (2003), these are likely to be conservative estimates for seasonal range because the full winter portion of the seasonal signal may not be represented. While warmer Permian summers could imply that icehouse summers were warmer than that today, warmer summers could also result from the influence of a large land mass in the Southern Hemisphere at this time (Crowley 1986), so long as portions of the continent were ice-free and so had lower albedo. The presence of plant fossils including large trees in this succession suggests this to be the case (Rees et al., 2002). In addition, we assume here that there is no seasonal change in the composition of local seawater, and this may not be the case. If there were some summer contribution from isotopically negative meltwater in the summers, the seasonal range of isotope values would be greater, giving the appearance of higher seasonality.

Table 2. Seasonal temperature range inferred for each region based on estimated water compositions and mean winter and summer $\delta^{18}O_{carb}$ values (assuming no change in water composition seasonally)

Region	**Range of water compositions (‰)**	**Mean winter $\delta^{18}O$ (‰)**	**Mean summer $\delta^{18}O$ (‰)**	**Temperature Range (°C)**
North Sydney Basin	-3.9 to -2.6	+0.60	-2.53	11-12
South Sydney Basin	-4.8 to -3.5	-0.32	-2.44	7-8
Tasmania Basin	-5.3 to -4.0	-0.79	-2.44	5-6

Conclusion

Although numerous authors have attempted to estimate temperatures from biogenic calcite in the high-latitudes of the Permian, each has recognized the same difficulty of estimating water compositions. The data presented in this research provide a method by which to better estimate water temperatures by constraining the latitudinal variability in water composition, a trend similar to that off of the coast of modern-day Greenland. By sampling individual specimens at a high-resolution, it is possible to recover the cyclic variability in $\delta^{18}O_{carb}$ that is indicative of seasonal temperature changes. Without constraints on the maximum and minimum compositions within specimens, it would be impossible to constrain winter minimum values that are necessary for our approach of estimating isotopic water compositions. Our results show that water compositions in the high-latitudes of SE Australia became as much as 1.4‰ more negative over 11° of increasing paleolatitude and 1,100 km of geographic spread. It may be possible to use this latitudinal gradient to better estimate temperatures from previously recovered specimens at similar paleolatitudes along SE Australia and even to help resolve the issue of seawater $\delta^{18}O$ for the Permian across all latitudes. Additional complicating factors such as seasonal run-off from highly-depleted meltwater sources must be taken into account as the amount of run-off is not likely to be equal year-round. Improved high-resolution sampling across a wider range of Permian paleolatitudes and geographical locations, as well as progress toward independent controls on paleotemperatures, may help better constrain Permian Ocean chemistry and climates.

Appendix

Table A1. Localities arranged by paleolatitude.

Locality	Paleolatitude	Formation	Age	Lithology	Fossils Present
Tangorin Core and Cranky Corner	64°S	Cranky Corner Sandstone	Middle-Late Sakmarian	massive green medium-fine grained sandstone	*Deltopecten*, *Megadesmus*, *Schizodus*, *Trigonotreta*, *Ingelarella*, *Suliciplica*, *Hyolithes*
Bimbadeen	64°S	Millfield Farm Formation (equivalent of the Allandale Fm)	Middle-Late Sakmarian	volcanogenic sands	*Deltopecten*, spiriferid brachiopods, bryozoans, crinoids, gastropods
Allandale RR Track	64°S	Allandale Formation	Middle-Late Sakmarian	conglomerate lithic sandstone	*Deltopecten*, *Megadesmus*, *Pyramus*, *Australomya*, *Schizodus*, spiriferid brachiopods, bryozoans, crinoids, gastropods
Wasp Head	68°S	Wasp Head Formation	Middle-Late Sakmarian	fine-medium grained sandstones and breccias	*Deltopecten*, *Megadesmus*, *Pyramus*, *Australomya*, *Schizodus*, *Ingelarella*, *Trigonotreta*, *Pseudosyrinx*, *Warthia*
North Head, Ulladulla	69°S	Wandrawandian Siltstone	Kungurian	Fine-grained quartz-lithic silty sandstone and siltstone	*Myonia*, productid and spiriferid brachiopods, *Thamnopora*(tabulate coral), crinoids and bryozoans
Maria Island	73°S	Darlington Limestone	Late Sakmarian	limestone with numerous layers of dropstones	*Deltopecten*, spiriferid brachiopods, numerous bryozoan types
Derwent River	75°S	Bundella Mudstone	Sakmarian	pebbly marine mudstone	*Deltopecten*, spiriferid brachiopods, rugose corals, crinoids

Australian Government, Geoscience Australia (http://dbforms.ga.gov.au/pls/www/geodx.strat_units.int) correspondence with Bruce Runnegar and Dan Petrizzo as well as; Runnegar, 1979, 1980b; McClung, 1980a; Ivany and Runnegar, 2010; Rygel et al., 2008; Fielding et al., 2006.

Table A2. Geochemical analyses

Locality	Basin	Sample Location	Mn ppm	Sr ppm	Mg ppm	Fe ppm
Allandale	NSB	Outer Region	3	403	1053	<5
Allandale	NSB	Central Region (sampling area)	2	372	969	<5
Allandale	NSB	Inner Region	3	378	1101	<5
Allandale	NSB	Outer Region	8	350	1048	<5
Allandale	NSB	Central Region (sampling area)	3	421	1332	<5
Allandale	NSB	Inner Region	2	454	1160	<5
Bimbadeen	NSB	Outer Region	54	406	1451	<5
Bimbadeen	NSB	Central Region (sampling area)	20	424	1280	<5
Bimbadeen	NSB	Inner Region	30	366	1087	<5
Bimbadeen	NSB	Outer Region	10	437	1189	<5
Bimbadeen	NSB	Central Region (sampling area)	11	513	1363	<5
Bimbadeen	NSB	Inner Region	8	413	1147	<5
Cranky Corner	NSB	Outer Region	12	479	1293	<5
Cranky Corner	NSB	Central Region (sampling area)	12	591	1670	54
Cranky Corner	NSB	Inner Region	36	479	1635	242
Cranky Corner	NSB	Outer Region	42	389	1259	<5
Cranky Corner	NSB	Inner Region	24	417	1287	74
Tangorin	SSB	Outer Region	6	364	1166	237
Tangorin	SSB	Central Region (sampling area)	5	455	1429	284
Tangorin	SSB	Inner Region	53	584	2088	345
North Head	SSB	Central Region (sampling area)	27	492	2042	<5
North Head	SSB	Inner Region(near microborings)	403	574	1833	970
Wasp Head	SSB	In "exterior texture"	4	490	1379	<5
Wasp Head	SSB	In "central" texture (towards central region)	5	520	1469	266
Wasp Head	SSB	in crack (inner portion) crack 1	170	453	1380	96
Wasp Head	SSB	adjacent to crack 1	6	340	1254	<5
Wasp Head	SSB	in crack (near edge) crack 2	17	455	1568	<5
Wasp Head	SSB	adjacent to crack 2	11	514	1879	<5
Wasp Head	SSB	Central Region (sampling area)	4	395	1248	<5
Maria Island	TS	In "exterior texture"	3	513	1482	245
Maria Island	TS	In "central" texture (sampled areas)	2	500	1300	188
Maria Island	TS	Potential cement?	434	1681	1434	7027
Maria Island	TS	Potential cement?	420	806	1543	4634
Maria Island	TS	Outer Region	5	517	1327	<5
Maria Island	TS	Central Region (sampling area)	1	371	1022	<5
Maria Island	TS	Inner Region	4	465	1600	<5
Maria Island	TS	In crack towards edge	93	938	1893	1712
Maria Island	TS	adjacent to crack	10	498	1301	223

Maria Island	TS	Transect (outer-most sample)	7	535	1285	62
Maria Island	TS	Transect	6	552	1330	135
Maria Island	TS	Transect	5	566	1363	259
Maria Island	TS	Transect	5	566	1323	171
Maria Island	TS	Transect	6	538	1462	256
Maria Island	TS	Transect	5	567	1431	400
Maria Island	TS	Transect	6	590	1546	309
Maria Island	TS	Transect	6	570	1571	391
Maria Island	TS	Transect	4	568	1565	299
Maria Island	TS	Transect	3	569	1578	322
Maria Island	TS	Transect	5	562	1694	377
Maria Island	TS	Transect (inner-most sample)	8	610	1934	432
Derwent River	SSB	Outer Region	63	421	1227	<5
Derwent River	SSB	Central Region (sampling area)	20	361	1011	<5
Derwent River	SSB	Inner Region	18	327	1186	<5
Derwent River	TS	Central Region (sampling area)	15	549	1697	403

Locality, sedimentary basin, sample ID, location of the sample within the specimen, and the corresponding values for Mn, Sr, Mg, and Fe (all in ppm). 'Central Region (sampling area)' denotes the region of the shell that was microsampled for stable isotopes. 'Outer Region' denotes a region of the shell near the exterior, 'Inner Region' is the region of the shell closest to the body cavity. Several other samples were taken within cracks and adjacent to the sampled cracks, and in regions that contained microborings. In addition to these, a transect was taken across one shell from Maria Island (MIs2A) from the exterior of the shell towards the interior to investigate the possibility of a trend with distance from the matrix.

Table A3. Stable isotope values of micromilled specimens, distances along the milled trajectory for each sample, and positions of growth bands.

Basin	distance (mm)	Specimen	$\delta^{18}O_{carb}$	$\delta^{13}C_{carb}$	Growth bands
NSB	0.000	ARR1C	0.54	6.07	y
	0.407	ARR1C	-1.29	5.96	
	0.815	ARR1C	-2.06	6.49	
	1.222	ARR1C	-2.74	6.89	
	1.629	ARR1C	-3.67	6.61	
	2.037	ARR1C	-2.34	5.92	
	2.572	ARR1C	0.15	6.01	y
	3.334	ARR1C	-0.87	6.07	
	3.838	ARR1C	-1.78	5.96	
	4.342	ARR1C	-2.06	6.23	
	4.845	ARR1C	-1.78	6.41	
	5.349	ARR1C	-1.67	6.32	
	5.853	ARR1C	0.65	6.27	
	6.104	ARR1C	0.05	6.11	y
	7.042	ARR1C	-1.90	5.99	
	8.150	ARR1C	-2.70	6.57	
	8.572	ARR1C	-2.73	6.84	
	8.994	ARR1C	-3.48	6.64	
	9.767	ARR1C	-0.50	6.90	
	10.179	ARR1C	0.63	6.43	
	10.454	ARR1C	-1.42	6.40	y
	11.128	ARR1C	-1.91	6.46	
	11.830	ARR1C	-2.20	6.38	

	12.339	ARR1C	-1.33	6.30	
	13.013	ARR1C	-1.43	6.28	
	13.745	ARR1C	0.35	6.28	
	14.218	ARR1C	0.05	6.13	y
NSB	0.000	Bimbadeen	-1.44	5.59	
	0.223	Bimbadeen	-1.80	5.56	
	0.446	Bimbadeen	-1.83	5.47	
	0.669	Bimbadeen	-1.72	5.63	
	0.892	Bimbadeen	-1.85	5.76	
	1.115	Bimbadeen	-1.96	5.72	
	1.338	Bimbadeen	-1.80	5.83	
	1.561	Bimbadeen	-1.12	6.10	
	1.784	Bimbadeen	-0.06	6.14	
	2.007	Bimbadeen	0.58	6.11	
	2.231	Bimbadeen	1.11	5.68	y
	2.454	Bimbadeen	0.98	5.53	
	2.677	Bimbadeen	0.14	5.38	
	2.900	Bimbadeen	-0.22	5.50	
	3.123	Bimbadeen	-1.22	5.60	
	3.346	Bimbadeen	-1.59	5.57	
	3.569	Bimbadeen	-2.28	5.60	
	3.792	Bimbadeen	-1.64	5.69	
	4.015	Bimbadeen	-2.43	5.45	
	4.238	Bimbadeen	-1.83	5.70	
	4.461	Bimbadeen	-1.63	5.83	
	4.684	Bimbadeen	-1.49	5.92	
	4.907	Bimbadeen	-0.52	6.21	

	5.130	Bimbadeen	0.24	6.18	
	5.353	Bimbadeen	0.74	5.80	y
	5.576	Bimbadeen	0.36	5.80	
	5.859	Bimbadeen	-0.73	5.75	
	6.089	Bimbadeen	-1.46	5.97	
	6.320	Bimbadeen	-1.34	5.77	
	6.551	Bimbadeen	-2.11	5.84	
	6.782	Bimbadeen	-1.79	6.04	
	7.013	Bimbadeen	-1.62	6.02	
	7.243	Bimbadeen	-2.32	6.05	
	7.474	Bimbadeen	-2.61	5.64	
	7.705	Bimbadeen	-2.11	5.94	
	7.936	Bimbadeen	-0.87	6.15	
	8.166	Bimbadeen	0.25	6.10	
	8.397	Bimbadeen	0.81	5.76	y
	8.628	Bimbadeen	-0.02	5.71	
	8.859	Bimbadeen	-0.65	5.73	
	9.090	Bimbadeen	-1.61	5.99	
	9.320	Bimbadeen	-1.87	5.96	
	9.551	Bimbadeen	-1.97	6.03	
	9.782	Bimbadeen	-2.90	6.14	
	10.013	Bimbadeen	-2.73	5.93	
	10.243	Bimbadeen	-2.73	5.84	
	10.474	Bimbadeen	-2.57	5.93	
	10.705	Bimbadeen	-1.30	6.05	
	10.936	Bimbadeen	0.40	6.01	
	11.167	Bimbadeen	0.91	5.96	y

	11.635	Bimbadeen	-0.96	5.57	
	11.883	Bimbadeen	-0.51	5.53	
	12.131	Bimbadeen	-1.14	5.52	
	12.379	Bimbadeen	-0.63	5.42	
	12.628	Bimbadeen	-1.48	5.64	
	12.876	Bimbadeen	-1.26	5.92	
	13.124	Bimbadeen	0.37	6.27	
	13.372	Bimbadeen	1.02	5.94	y
	13.621	Bimbadeen	0.59	5.39	
	13.869	Bimbadeen	-0.53	5.53	
	14.117	Bimbadeen	-0.50	5.58	
	14.366	Bimbadeen	-0.97	5.40	
	14.614	Bimbadeen	-1.65	5.72	
	14.862	Bimbadeen	-2.01	5.91	
	15.110	Bimbadeen	-2.58	6.06	
	15.359	Bimbadeen	-1.59	6.32	
	15.607	Bimbadeen	0.32	6.56	
	15.855	Bimbadeen	1.03	6.15	y
	16.103	Bimbadeen	0.93	5.70	
	16.352	Bimbadeen	-0.18	5.64	
NSB	0.000	Tangorin	-1.55	4.52	y
	0.246	Tangorin	0.87	4.82	
	0.491	Tangorin	0.63	5.06	
	0.864	Tangorin	-0.66	4.38	
	1.135	Tangorin	-1.02	3.82	
	1.688	Tangorin	-1.62	3.63	y
	1.988	Tangorin	-0.42	4.35	

	2.159	Tangorin	0.73	4.62	
	2.331	Tangorin	0.07	4.42	
	2.502	Tangorin	-0.53	4.30	
	2.674	Tangorin	-0.91	3.88	
	2.845	Tangorin	-1.10	3.55	
	3.016	Tangorin	-0.50	3.88	
	3.543	Tangorin	0.26	4.15	
	4.172	Tangorin	-0.05	3.92	y
	4.293	Tangorin	-0.38	3.85	
	4.415	Tangorin	-0.64	3.78	
	4.536	Tangorin	-0.40	4.08	
	4.829	Tangorin	-0.26	3.98	
	5.122	Tangorin	-0.11	3.99	
	5.415	Tangorin	-0.82	3.78	
	5.708	Tangorin	-1.03	3.61	
	6.001	Tangorin	-0.61	3.81	
	6.959	Tangorin	0.17	4.18	y
	7.781	Tangorin	0.24	3.99	
	7.945	Tangorin	-0.57	3.79	
	8.110	Tangorin	-1.22	3.51	
	8.275	Tangorin	-1.52	3.43	
	8.439	Tangorin	-1.25	3.63	
	8.604	Tangorin	-0.14	4.09	y
NSB	0.000	CC1D	-1.19	4.82	
	0.365	CC1D	0.80	5.01	y
	0.865	CC1D	-0.01	4.70	
	1.056	CC1D	-0.64	4.84	

	1.422	CC1D	-0.73	4.94	
	1.610	CC1D	-1.20	4.90	
	1.797	CC1D	-1.33	4.87	
	1.984	CC1D	-1.08	5.08	
	2.503	CC1D	-0.90	5.22	
	2.681	CC1D	0.91	5.13	y
	2.859	CC1D	0.13	4.42	
	3.037	CC1D	-0.79	4.53	
	3.215	CC1D	-0.89	4.58	
	3.393	CC1D	-1.14	4.79	
	3.571	CC1D	-1.17	4.98	
	3.749	CC1D	-1.07	5.21	y
	3.887	CC1D	0.49	4.58	
	4.025	CC1D	-0.27	4.45	
	4.163	CC1D	-0.72	4.43	
	4.301	CC1D	-1.28	4.59	
	4.438	CC1D	-1.39	4.66	
	4.576	CC1D	-1.27	4.73	
	4.714	CC1D	-1.38	4.79	y
	4.848	CC1D	0.08	4.65	
	4.981	CC1D	0.04	4.18	
	5.115	CC1D	-0.62	4.16	
	5.248	CC1D	-0.89	4.41	
	5.382	CC1D	-0.78	4.50	
	5.515	CC1D	-0.44	4.84	
	5.649	CC1D	0.61	5.13	y
	5.787	CC1D	0.95	4.43	

	5.926	CC1D	-0.26	3.93	
	6.065	CC1D	-0.64	4.18	
	6.203	CC1D	-0.89	4.42	
	6.342	CC1D	-0.96	4.55	
	6.481	CC1D	-1.40	4.42	
	6.619	CC1D	-1.59	4.36	y
SSB	0.000	WH1A	0.81	4.85	y
	0.292	WH1A	-0.28	4.50	
	0.712	WH1A	0.20	4.70	
	1.371	WH1A	-1.31	4.89	
	1.663	WH1A	-1.40	4.53	
	1.956	WH1A	-1.95	4.87	
	2.592	WH1A	-1.33	4.84	
	2.897	WH1A	-1.75	4.71	
	3.250	WH1A	-0.63	5.20	y
	3.521	WH1A	0.19	4.61	
	3.792	WH1A	-0.63	4.97	
	4.062	WH1A	-0.68	4.85	
	4.333	WH1A	-1.49	4.99	
	4.604	WH1A	-2.20	4.85	
	4.874	WH1A	-2.15	5.08	
	5.145	WH1A	-1.72	5.22	y
	5.823	WH1A	-0.24	4.88	
	6.326	WH1A	-0.67	5.16	
	6.631	WH1A	-1.28	5.07	
	6.936	WH1A	-1.30	5.09	
	7.352	WH1A	-0.15	5.09	

	8.037	WH1A	-1.95	5.26	
	8.342	WH1A	-1.36	5.08	y
	8.588	WH1A	-2.39	4.75	
	9.258	WH1A	-0.62	4.94	
	9.877	WH1A	-0.12	4.74	
	10.123	WH1A	0.55	4.68	
	10.369	WH1A	-0.74	5.29	
	10.615	WH1A	-3.82	4.33	
	11.103	WH1A	-2.67	5.18	y
SSB	0.000	NH1C	-1.22	4.96	y
	0.284	NH1C	-1.14	5.40	
	0.568	NH1C	-2.21	4.58	
	1.021	NH1C	-1.69	4.89	
	1.300	NH1C	-1.92	4.81	
	1.579	NH1C	-1.89	5.11	
	2.179	NH1C	-3.06	4.59	y
	2.463	NH1C	-2.34	5.04	
	2.757	NH1C	-2.35	5.08	
	3.051	NH1C	-2.28	5.02	
	4.522	NH1C	-0.68	5.62	y
	4.872	NH1C	-1.30	5.31	
	5.468	NH1C	-0.77	5.21	y
	5.822	NH1C	-1.41	4.86	
	6.175	NH1C	-2.59	4.61	
	6.528	NH1C	-1.82	5.16	
	6.881	NH1C	-2.08	5.08	
	7.742	NH1C	-1.97	5.04	

	8.092	NH1C	-1.58	5.00	
	9.325	NH1C	-0.89	5.35	y
TS	0.000	MIsA	-1.51	5.64	y
	0.238	MIsA	-1.48	5.83	
	0.504	MIsA	-2.61	5.60	
	0.769	MIsA	-2.89	5.60	
	1.034	MIsA	-3.08	5.25	
	1.299	MIsA	-2.67	5.33	
	1.565	MIsA	-2.22	5.15	
	1.830	MIsA	-1.44	5.33	
	2.267	MIsA	-1.14	5.56	y
	2.542	MIsA	-1.60	5.42	
	2.817	MIsA	-2.63	5.18	
	3.093	MIsA	-2.48	5.22	
	3.368	MIsA	-2.32	5.11	
	3.643	MIsA	-1.97	4.88	
	3.919	MIsA	-1.71	4.95	y
	4.749	MIsA	-0.89	5.44	
	5.488	MIsA	-1.06	5.58	
	5.780	MIsA	-2.28	5.04	
	6.288	MIsA	-2.15	5.09	
	6.994	MIsA	-2.43	4.89	
	7.286	MIsA	-2.55	4.75	
	7.792	MIsA	-1.67	4.94	
	8.330	MIsA	-0.57	5.12	y
	8.628	MIsA	-1.02	5.19	
	9.101	MIsA	-2.02	5.18	

	9.407	MIsA	-2.49	5.19	
	10.163	MIsA	-2.21	5.30	
	10.655	MIsA	-2.32	5.38	
	10.961	MIsA	-1.68	4.76	
	11.268	MIsA	-1.03	4.63	
	12.052	MIsA	-0.82	5.13	y
	12.346	MIsA	-0.97	4.98	
	12.914	MIsA	-1.58	4.72	
	13.222	MIsA	-2.47	4.74	
	13.529	MIsA	-2.14	4.68	
	13.836	MIsA	-0.80	4.45	y
TS	0.000	MIs2B	-1.05	4.77	y
	0.345	MIs2B	-0.98	4.62	
	0.689	MIs2B	-2.15	4.98	
	1.034	MIs2B	-2.39	5.06	
	1.379	MIs2B	-2.33	4.82	
	1.723	MIs2B	-2.26	4.74	
	2.068	MIs2B	-1.95	4.69	
	2.413	MIs2B	-0.84	5.21	y
	2.717	MIs2B	-0.57	4.86	
	3.020	MIs2B	-1.56	4.93	
	3.324	MIs2B	-1.64	5.07	
	3.628	MIs2B	-2.05	4.79	
	3.932	MIs2B	-2.24	4.53	
	4.235	MIs2B	-1.58	4.73	
	4.539	MIs2B	-0.46	5.12	y
	4.822	MIs2B	-1.92	5.12	

	5.104	MIs2B	-2.11	4.95	
	5.387	MIs2B	-2.02	4.80	
	5.669	MIs2B	-2.06	4.77	
	5.952	MIs2B	-1.71	4.64	
	6.234	MIs2B	-0.69	5.06	
	6.547	MIs2B	-0.95	4.65	y
	6.859	MIs2B	-1.96	4.99	
	7.171	MIs2B	-2.17	5.10	
	7.483	MIs2B	-2.52	4.93	
	7.796	MIs2B	-2.19	4.68	
	8.108	MIs2B	-1.55	4.77	
	8.420	MIs2B	-0.12	4.79	y
	8.703	MIs2B	-0.95	4.68	
	8.986	MIs2B	-1.67	4.70	
	9.269	MIs2B	-2.23	4.59	
	9.552	MIs2B	-1.70	4.56	
	9.834	MIs2B	-0.65	4.94	y
	10.117	MIs2B	-1.07	4.75	
TS	0.000	DR1B	-4.00	4.75	y
	0.428	DR1B	-4.10	5.00	
	0.856	DR1B	-4.25	5.03	
	1.383	DR1B	-4.28	4.99	
	1.796	DR1B	-4.15	5.08	
	2.210	DR1B	-5.09	4.58	
	2.624	DR1B	-4.69	4.36	
	3.158	DR1B	-3.29	4.75	y
	3.558	DR1B	-3.07	4.87	

	3.813	DR1B	-4.09	4.83	
	4.323	DR1B	-3.56	5.12	
	4.750	DR1B	-4.05	5.08	y
	5.797	DR1B	-3.61	4.68	
	6.225	DR1B	-3.83	4.48	
	6.566	DR1B	-3.14	4.77	y
	7.750	DR1B	-3.45	4.94	
	8.192	DR1B	-2.99	4.92	
	8.976	DR1B	-2.90	4.79	
	9.474	DR1B	-3.61	4.77	
	10.354	DR1B	-4.01	5.01	y

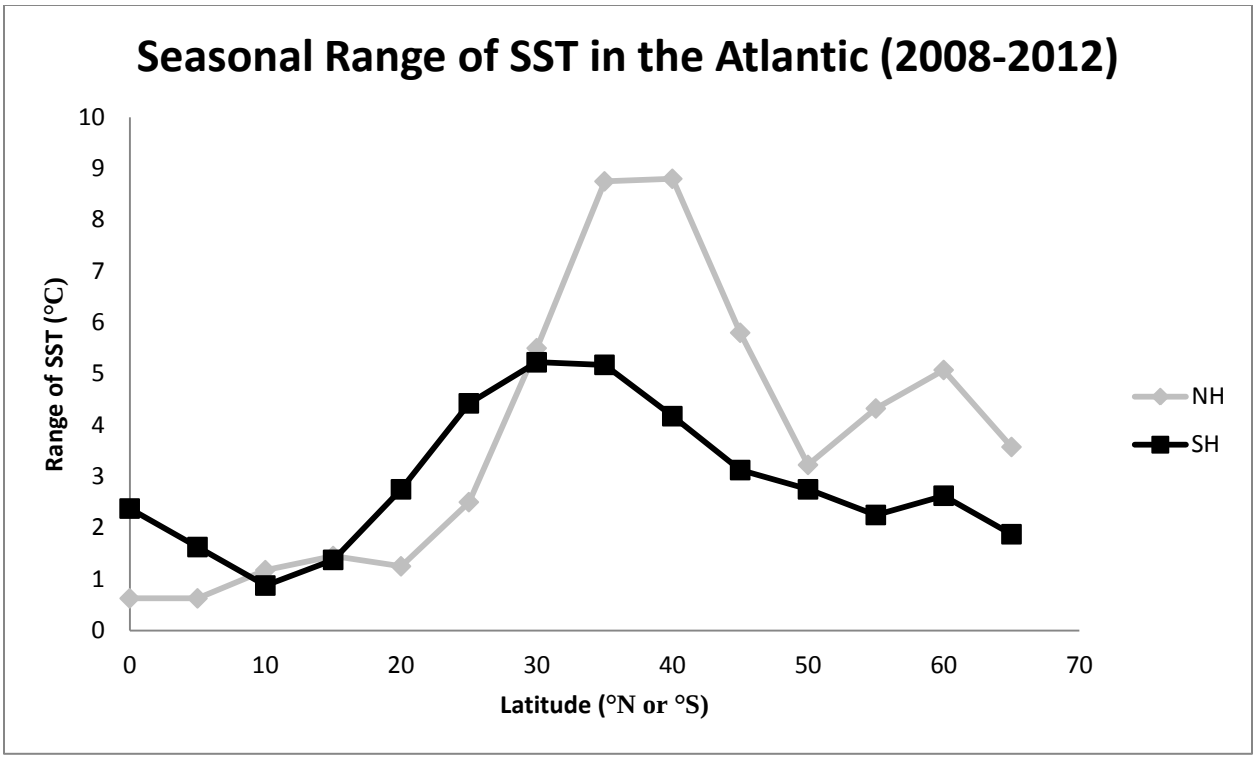

Figure A1) Plot of the seasonal range of temperatures from the Northern and Southern Hemispheres for the modern Atlantic Ocean. The range of SST is computed from the difference between average SST for the months of January and August, from August 2008 to January 2012. Maximum seasonality is achieved at the mid-latitudes in both the northern and southern hemispheres of the Atlantic Ocean, with seasonality decreasing in both directions away from the mid-latitudes. Data downloaded from the NASA Earth Observations Website at http://neo.sci.gsfc.nasa.gov/Search.html?group=10.

References

Anderson, T.F., and M.A. Arthur, 1983. Stable isotopes of oxygen and carbon and their application to sedimentological and paleoenvrionmental problems. In M.A. Arthur, T.F. Anderson, I.R. Kaplan, J. Veizer, and L. Land, eds., Stable isotopes in sedimentary geology, SEPM Short Course, 10: 1-151.

Angiolini, L, Jadoul, F, Leng, M.J., Stephenson, M.H., Rushton, J., Chenery, S. and C. Crippa, 2009. How cold were the Early Permian glacial tropics? Testing sea-surface temperature using the oxygen isotope composition of rigorously screened brachiopod shells. Journal of the Geological Society 166: 933-945.

Australian Government, Geoscience Australia. (2011, February 4). *Australian Government*. Retrived March 15, 2011, from Geoscience Australia Web site: http://dbforms.ga.gov.au/www/geodx.strat_units.int

Bischoff, J.L., Fitzpatrick, J.A., and R.J. Rosenbauer, 1993. The solubility and stabilization of ikaite ($CaCO_3$*$6H_2O$) from 0° to 25°C: Environmental and Paleoclimatic implications for thinolite tuffa. Journal of Geology 101: 21-33.

Brand, U., 1989. Biogeochemistry of late Paleozoic North American brachiopods and secular variation of seawater composition. Biogeochemistry 7: 159– 193.

Brand, U., Logan, A., Hiller, and J. Richardson, 2003. Geochemistry of modern brachiopods: applications and implications for oceanography and paleoceanography. Chemical Geology 198: 305– 334.

Brand, U., 2004. Carbon, oxygen and strontium isotopes in Paleozoic carbonate components: an evaluation of original seawater-chemistry proxies. Chemical Geology, 204: 23-44.

Buick, D., and L. Ivany. 2004, 100 years in the dark; extreme longevity of Eocenc bivalves from Antarctica. Geology 32: 921-924.

Carter, J.G., and F.G. Stehli, 1980. Environmental and biological controls of bivalve shell mineralogy and microstructure, in C.C. Rhoads, and R.A. Lautz, eds., Skeletal Growth of Aquatic Organisms: biological records of environmental change: New York Plenum Press, p. 69-113.

Clapham, M.E. and P.J. James, 2008. Paleoecology of Early-Middle Permian marine communities in Eastern Australia: Response to global climate change in the aftermath of the Late Paleozoic Ice Age. PALAIOS 23(11): 738-750.

Compston, W., 1960. The carbon isotopic compositions of certain marine invertebrates and coals from the Australian Permian. Geochimica et Cosmochimica Acta 18: 1–22.

Crowley, T.J., Short, D.A., Mengel, J.G., and G.R. North, 1986. Role of Seasonality in the Evolution of Climate during the Last 100 Million Years. Science. 231: 579-584

De Lurio, J. L. and L. A. Frakes, 1999. Glendonites as a paleoenvironmental tool: Implications for early Cretaceous high latitude climates in Australia. Geochemica et Cosmochimica 63: 1039-1048.

Dickins, J.M., 1978, Climate of the Permian in Australia: The invertebrate faunas: Palaeogeography, Palaeoclimatology, Palaeoecology, v. 23, p. 33–46, doi: 10.1016/0031-0182(78)90080-9.

Dickins, J.M., 1996, Problems of a late Palaeozoic glaciation in Australia and subsequent climate in the Permian: Palaeogeography, Palaeoclimatology, Palaeoecology, v. 125, p. 185–197, doi: 10.1016/S0031-0182(96)00030-2.

Ekwurzel, B., P. Schlosser, R. A. Mortlock, R. G. Fairbanks, and J. H. Swift, 2001. River runoff, sea ice meltwater, and Pacific water distribution and mean residence times in the Arctic Ocean. Journal of Geophysical Research 106(c5):9075-9092.

Epstein, S., Buchsbaum, H.S., Lowenstam, H.A., and H.C. Urey, 1953. Revised carbonate-water isotopic temperature scale: Geological Society of America Bulletin, v. 64, p. 1315–1326, doi: 10.1130/0016-7606(1953)64[1315: RCITS]2.0.CO;2

Fielding, C., Bann, K., Macearchern, J., Tye, S., and B. Jones, 2006. Cyclicity in the nearshore marine to coastal, Lower Permian, Pebbley Beach Formation, southern Sydney Basin, Australia: a record of relative sea-level fluctuations at the close of the Late Paleozoic Gondwanan ice age. Sedimentology 53: 435-463.

Fielding, C., Frank, T., Birgenheier, L., Rygel, M., Jones, A., and J. Roberts, 2008. Stratigraphic imprint of the Late Palaeozoic Ice Age in eastern Australia: a record of alternating glacial and nonglacial climate regime. Journal of the Geological Society 165: 129-140.

Fielding, C., Frank, T., Isbell, J., Henry, L., and E. Domack, 2010. Stratigraphic signature of the late Palaeozoic Ice Age in the Parmeener Supergroup of Tasmania, SE Australia, and inter-regional comparisons. Paleogeography, Paleoclimatology, Paleoecology: 298: 70-90.

Frank, T.D., Montañez, I.P., Fielding, C.R., and M.C. Rygel, 2008a. Late Paleozoic climate dynamics revealed by comparison of ice-proximal stratigraphic and ice-distal isotopic records. The Geological Society of America Special Paper 441: 331-342.

Frank, T.D., Thomas, S. G. and C. R. Fielding, 2008b. On using carbon and oxygen isotope data from glendonites as paleoenvironmental proxies: A case study from the Permian system of Eastern Australia. Journal of Sedimentary Research 78: 713-723.

Goodwin, D. H., B. R. Schone, and D. L. Dettman, 2003. Resolution and fidelity of oxygen isotopes as paleotemperature proxies in bivalve mollusk shells: Models and observations. Palaios 18:110-125.

Grossman, E., Yancey, T., Jones, T., Bruckschen, P., Chuvashov, B., Mazzullo, S., and Hong-shen Mii, 2008. Glaciation, ardification, and carbon sequestration in the Permo-Carboniferous: The isotopic record from low latitudes. Paleogeography, Paleoclimatology, Paleoecology 268: 222-233.

Hallmann, N., Schöne, B.R., Strom, A., and J. Fiebig, 2008. An intractable climate archive-Sclerochronological and shell oxygen isotope analyses of the Pacific geoduck. *Panopea abrupt* (bivalve mollusk) fom Protection Island (Washington State, USA). Paleogeography, Paleoclimatology, Paleoecology 269: 115-126.

Herbert, C., 1980. Depositional Development of the Sydney Basin, *in* Herbet, C., and Helby, R., eds., A guide to the Sydney basin. Geological Survey of New South Wales Bulletin 26: 10-52.

Ivany, L.C. and B. Runnegar, 2010. Early Permian seasonality from bivalve $\delta^{18}O$ and implications for the oxygen isotopic composition of seawater. Geology 38: 1027-1030.

Ivany, L., Wilkinson, B., Lohmann, K., Johnson, E., McElroy, B., and G. Cohen, 2004. Intra-annual isotopic variation in Venericardia bivalves; implications for early Eocene temperature, seasonality, and salinity on the U.S. Gulf Coast. Journal of Sedimentary Research 74: 7-19.

Jaffrés. J.B.D., Shiels, G.A., and K. Wallmann, 2007. The oxygen isotope evolution of seawater: A critical review of a long-standing controversy and an improved geological water cycle model for the past 3.4 billion years. Earth-Science Reviews 83: 83-122.

James, N.P., Frank, T.D., and C.R. Fielding. 2009. Carbonate sedimentation in a Permian high-latitude subpolar depositional realm: Queensland, Australia. Journal of Sedimentary Research 79: 125-143.

Jones, D.S., 1980 Annual cycle of shell growth increment formation in two continental shelf bivalves and its paleoecologic significance. Paleobiology 6(3): 331-340.

Klein, R., Lohmann, K., and C. Thayer, 1996. Bivalve skeletons record sea-surface temperature and $\delta^{18}O$ via Mg/Ca and $^{18}O/^{16}O$ ratios. Geology 24: 415-418.

Korte, C., Jasper, T., Kozur, and J. Veizer. 2005. $\delta^{18}O$ and $\delta^{13}C$ of Permian brachiopods: A record of sweater evolution and continental glaciation. Paleogeography, Paleoclimatology, Paleoecology 224: 333-351.

Korte, C., Jones, P.J., Brand, U., Mertmann, D., and J. Veizer, 2008. Oxygen isotope values from high-latitudes: clues for Permian sea-surface temperature gradients and Late Palaeozoic deglaciation. Paleogeography, Paleoclimatology, Paleoecology 269: 1-16.

LeGrande, A.N., and G.A. Schmidt, 2006: Global gridded data set of the oxygen isotopic composition in seawater. *Geophys. Res. Lett.*, **33**, L12604, doi:10.1029/2006GL026011.

Li, Z. and C. Powell, 2001. An outline of the palaeogeographic evolution of the Australasian region since the beginning of the Neoproterozoic. Earth Science Review 53: 237-277.

Lohmann, K. C. and C. G. Walker. 1989. The $\delta^{18}O$ record of Phanerozoic abiotic marine calcite cements. Geophysical Research Letters 16: 319-322.

Lowenstam, H.A., 1961. Mineralogy, O^{18}/O^{16} ratios, and strontium and magnesium contents of Recent and fossil brachiopods and their bearing on the history of the oceans. Journal of Geology 69 (3): 241–260.

McClung, G., 1980a. Permian Biostratigraphy of the northern Sydney basin, in Herbert C., and Helby, R., eds., A guide to the Sydney basin. Geological Survey of New South Wales Bulletin 26: 361-375.

-, 1980b. Permian marine sedimentation, northern Sydney basin. Geological Survey of New South Wales Bulletin 26: 54-72.

Mii, H.S., and E.L. Grossman, 1994. Late Pennsylvanian seasonality reflected in the $\delta^{18}O$ of a brachiopod shell. Geology 22: 661-664.

Mii, H.S., and , E.L. Grossman, 1997. Stable carbon and oxygen isotope shifts in Permian seas of West Spitsbergen- Global change of diagenetic artifact? Geology, 25: 227-230.

Mii, H.S., Shi, G.R., Cheng, C., and Yun-Yung Chen, 2012. Permian Gondwanaland paleoenvironment inferred from carbon and oxygen isotope records of brachiopod shells from Sydney Basin, southeast Australia. Chemical Geology 291: 87-103.

Mook, W., and J. Vogel, 1968., Isotopic Equilibrium between shells and Their Environment. Science 159: 874-875.

Morante, R., 1996., Permian and Early Triassic isotopic records of carbon and strontium in Australia and a scenario of events about the Permian–Triassic boundary. Historical Biology 11: 289–310.

Morrison, J.O. and U. Brand, 1986. Geochemistry of recent marine invertbrtes. Geoscience Canada 19(4): 237-254.

NASA Earth Observations, National Aeronautics and Space Administration (2012, May 10) Retrieved March 1, 2012 from NEO website: http://neo.sci.gsfc.nasa.gov/Search.html?group=10

Nützel, A., Joachimski, M. and M. L. Correa, 2010. Seasonal climatic fluctuations in the late Triassic tropics-High-resolution oxygen isotope records from an aragonitic bivalve shells (Cassian Formation, Northern Italy). Paleogeography, Paloeclimatology, Paleoecology 285 : 194-204.

Quitmeyer, I.R., Hale, H.S., and D.S. Jones, 1985. Paleoseasonality determination based on incremental shell growth in the hard clam *Mercernaria mercenaria*, and its implications

for the analysis of three southeast Georgia coastal shell middens. Southeastern Archaeology 4(1): 24-40.

Rees, P.M., Ziegler, A.M., Gibbs, M.T., Kutzbach, J.E., Behling, P.J., and D.B. Rowley, 2002, Permian phytogeographic patterns and climate data/model comparisons. Journal of Geology, v. 110, p. 1–31, doi: 10.1086/324203.

Reid, C. M., and N. P. James, 2010. Permian higher latitude bryozoan biogeography. Paleogeography, Paloeclimatology, Paleoecology 298 : 31-41.

Reid, C.M., 2010. Environmental controls on the distribution of Late Paleozoic bryozoan colony morphotypes: An example from the Permian of Tasmania, Australia. Palaios 25: 692-702.

Rickaby, R., Shaw, S., Bennitt, G., Kennedy, H., Zabel, M., and A. Lennie, 2006. Potential of ikaite to record the evolution of oceanic $\delta^{18}O$. Geology 34: 497-500.

Runnegar, B., 1979. Ecology of *Eurydesma* and the *Eurydesma* fauna, Permian of eastern Australia. Alcheringa 3: 261-285.

Runnegar, B., 1980a. Marine Shoalhaven group, southern Sydney basin, in Herbert C., and Helby, R., eds., A guide to the Sydney basin. Geological Survey of New South Wales Bulletin 26: 74-81.

-, 1980b. Biostratigraphy of the Shoalhaven group. Geological Survey of New South Wales Bulletin 26: 377-382.

Rygel, M.C., Fielding, C.R., Bann, K.L., Frank, T.D., Birgenheier, L., and S.C. Tye, 2008. The Lower Permian Wasp Head Formation, Sydney Basin: high-latitude, shallow marine sedimentation following the late Asselian to early Sakmarian glacial event in eastern Australia. Sedimentology 55: 1517-1540.

Sato-Okoshi, W., and K. Okoshi, 2007. Characteristics of shell microstructure and growth analysis of the Antarctic bivalve *Laternula elliptica* from Lützow-Holm Bay, Antarctica. Polar Biology 31(2):131-138.

Schmidt, G.A., G. R. Bigg and E. J. Rohling, 1999. "Global Seawater Oxygen-18 Database - v1.21" http://data.giss.nasa.gov/o18data/

Schöne, B.R., Freyre Castro, A.D., Fiebig, J., Houk, S.D., Oschmann, W., and I. Kröncke, 2004. Sea surface water temperatures over the period 1884-1983 reconstructed fom oxygen isotope ratios of a bivalve mollusk shell (*Artica islandica*, southern North Sea). Paleogeography, Paleoclimatology, Paleoecology 212: 215-232.

Schöne, B.R., Houk, S.D., Freyre Castro, A.D., Fiebig, J., Oschmann, W., Kröncke, I., Dreyer, W., and F. Gosselck, 2005a. Daily Growth Rates in Shells of *Arctica islandica*: Assessing Sub-seasonal Environmental Controls on a Long-lived Bivalve Mollusk. PALAIOS 20(1): 78-92.

Schöne, B.R., Fiebig, J., Pfeiffer, M., Gleβ, R., Hickson, J., Johnson, A.L.A., Dreyer, W., and W. Oshmann, 2005b. Climate records from a bivalve Methuselah (*Arctica islandica*, Mollusca; Iceland). Paleogeography, Paleoclimatology, Paleoecology 228: 130-148.

Schöne, B., 2008. The curse of physiology-challenges and opportunities in the interpretation of geochemical data from mollusk shells. Geo-Marine Letters 28: 269-285.

Scotese, C.R. 1997. The Paleomap Project: paleogeographic atlas and plate tectonics software. Department of Geology, University of Texas, TX

Selleck, B.W., Carr, P.F., and B.G. Jones. 2007. A review and synthesis of glendonites (pseudomorphs after ikaite) with new data: assessing applicability as recorders of ancient coldwater conditions. 77: 980-991.

Stampfli, G. and G. Borel, 2002. A plate tectonic model for the Paleozoic and Mesozoic constrained by dynamic plate boundaries and restored synthetic oceanic isochrons. Earth and Planetary Science Letters 196: 17-33.

Suess, E., Balzer, W., Hesse, K., Muller, P., Ungerer, C., and G. Wefer, 1982. Calcium Carbonate Hexahydrate from Organic-Rich Sediments of the Antarctic Shelf: Precursors of Glendonites. Science 216: 1128-1131.

Veizer, J. Bruckschen, P., Pawellek, F., Diener A., Podlaha, O.G., Carden, G.A.F., Jasper, T., Korte, C., Strauss, H., Azmy, K., and D. Ala, 1997. Oxygen isotope evolution of Phanerozoic seawater. Paleogeography, Paleoclimatology, Paleoecology 132: 159-172.

Veizer, J., Ala, D., Azmy, K., Bruckschen, P., Buhl, D., Bruhn, F., Carden, G.A.F., Diener, A., Ebneth, S., Godderis, Y., Jasper, T., Korte, C., Pawellek, F., Podlaha, O.G., and H. Strauss, 1999. 87Sr/86Sr, δ13C and δ18O evolution of Phanerozoic seawater. Chemical Geology 161: 59-88.

Wenzel, B., Lêcuyer, C., and M. Joachimski, 2000. Comparing oxygen isotope records of Silurian calcite and phosphate-$\delta^{18}O$ compositions of brachiopods and conodonts. Geochemica et Cosmochimica Acta 64: 1859-1872.

Wenzel, B., 2000. Differential preservation of primary isotopic signatures in Silurian brachiopods from northern Europe. Journal of Sedimentary Research 70: 194-209.

Wilkinson, B., and L. Ivany, 2002. Paleoclimatic inference from stable isotope profiles of accretionary biogenic harparts; a quantitative approach to the evaluation of incomplete data. Paleogeography, Paleoclimatology, Paleoecology 185: 95-14.

Williams, D.F., Arthur, M.A., Jones. D.S., and N. Healy-Williams, 1982. Seasonality and mean annual sea surface temperatures from isotopic and sclerochronological records. Nature 296: 432-434.

Zachos, J.C., Stott, L.D. and K.C. Lohmann, 1994. Evolution of early Cenozoic marine temperatures. Paleoceanography 9 (2): 353-387

Vita

Education:

B.S. Geology University of Tennessee at Chattanooga (Chattanooga, TN) May 2010

Cumulative GPA: 3.186 GPA in Geology: 3.322
Senior Research: *Comparison of Brachiopod Genera from the Silurian Rockwood Formation in Tiftonia, Hamilton County, TN*

Teaching Experience:

-Earth Science (Course number: EAR 105)

Recitation Instructor 2 semesters and TA coordinator 1 semester. Course for non-majors. Responsibilities included: Basic instruction of coursework for each assignment, preparation of class materials and assignments, grading, designing recitations, distributing class materials to the other TAs and proctoring exams.

-History of Life (Course number: EAR 102)

Lab instructor and TA coordinator. This is a course for Earth Science majors and is an equivalent for most Historical Geology classes at other institutions. Duties for this class included helping to organize labs and lab materials, preparing the labs each week and coordinating field trips.

-Paleobiology Lab (Course number: EAR 325)

Lab Instructor. This is a writing intensive course required for Earth Science majors. Responsibilities included: Basic instruction for each lab, creating and organizing lab assignments, projects, quizzes and lab final exam, preparation and organization of lab materials and grading.

-Branson Field Laboratory 2011 (Field Camp in Lander, WY, ran by The University of Missouri at Columbia)

Teaching Assistant. Six week field experience course required for most majors in Geology. Responsibilities included: Grading, organizing teaching materials, field instruction and assisting students with assignments.

Honors, Awards, and Memberships:

- Lebron Carver Geology Scholarship: 2009 ($750.00)
-Tennessee Lottery Scholarship: 2005-2010 ($4000.00)
-UTC Dean's List (semester GPA of 3.20 or higher): multiple times
- Geological Society of America (student member)

- The Paleontological Society of America (student member)
- The Paleontological Society of America Student Research Grant ($800.00)
-Syracuse Earth Sciences Summer Award (Summer 2011)